CHALMERS
UNIVERSITY OF TECHNOLOGY

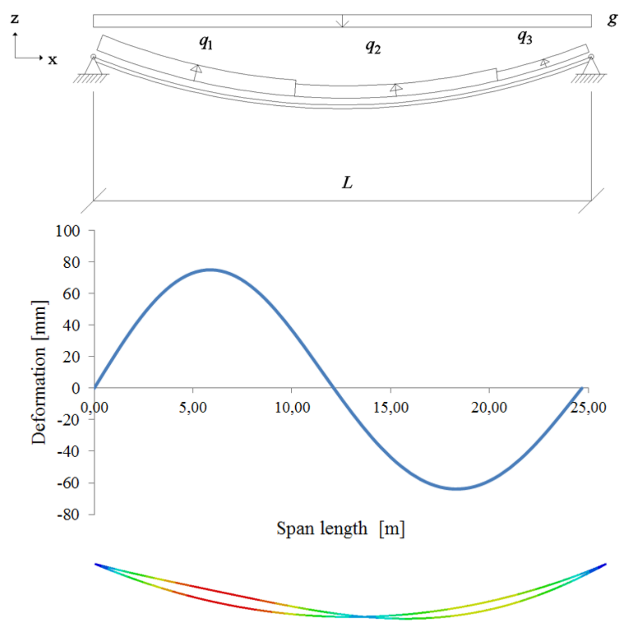

Application of Asymmetric Loads on Cable Shaped Structures

A load case study of Timber roof Stress Ribbon structures

Master's Thesis in the Master's Programme Structural Engineering and Building Technology

DAVID GUSTAFSSON
MARTIN INGVARSSON

Department of Civil and Environmental Engineering
Division of Structural Engineering
CHALMERS UNIVERSITY OF TECHNOLOGY
Gothenburg, Sweden 2017
Master's Thesis 2017:23

MASTER'S THESIS 2017:23

Application of Asymmetric Loads on Cable Shaped Structures

A load case study of Timber roof Stress Ribbon structures

Master's Thesis in the Master's Programme Structural Engineering and Building Technology

DAVID GUSTAFSSON
MARTIN INGVARSSON

Department of Civil and Environmental Engineering
Division of Structural Engineering
CHALMERS UNIVERSITY OF TECHNOLOGY

Gothenburg, Sweden 2017

Application of Asymmetric Loads on Cable Shaped Structures
A load case study of Timber roof Stress Ribbon structures
DAVID GUSTAFSSON
MARTIN INGVARSSON

Master's Thesis 2017:23
ISSN 1652-8557
Department of Civil and Environmental Engineering
Division of Structural Engineering
Chalmers University of Technology
SE-412 96 Gothenburg
Sweden
Telephone: +46 (0)31-772 1000

Colophon:
The thesis was created using LaTeX 2_ε and biblatex and edited on www.sharelatex.com. The typesetting software was the TeX Live distribution. The text is set in Times New Roman. Graphs were creating using PGFPLOTS and MS Excel. Figures were created using INKSCAPE.

Chalmers Reproservice
Gothenburg, Sweden 2017

Application of Asymmetric Loads on Cable Shaped Structures
A load case study of Timber roof Stress Ribbon structures
Master's Thesis in the Master's Programme Structural Engineering and Building Technology
DAVID GUSTAFSSON
MARTIN INGVARSSON
Department of Civil and Environmental Engineering
Division of Structural Engineering
Chalmers University of Technology

ABSTRACT

In the construction industry, the environmental impact has been an important issue over the recent years. The aim of decreasing the carbon dioxide emissions has increase the use of more sustainable material choices. The use of timber has a number of sustainable advantages e.g. the low self-weight and it binds carbon dioxide through its photosynthesis process. Reduce of the material consumption is also important in order to achieve a more sustainable structure.

In this thesis, long-span timber roof structures has been investigated. Using timber as the primary structural load carrying material has been studied. In order to achieve the material efficiency of the timber, a cable-like behaviour, further called stress ribbon, has been investigated.

The aim of the thesis is to investigate how asymmetric load affect the stress ribbon structure. Different load combinations induced by snow- and wind has been analysed and designed according to Eurocode. In order to design the stress ribbon structure for realistic load cases, an analytical and a numerical method has been carried out. Both ultimate limit state and serviceability limit state has been used for designing the stress ribbon structure.

A comparison of the analytical and the numerical solution for symmetric- and asymmetric load has been studied. The results for the asymmetric load case correspond well while for the symmetric load case the deflection and moment distribution have some deviation.

Finally the cable was designed for realistic load combinations were the snow and wind load was designed separately. The reason for this is that the wind gives suction all over the roof. The results from the snow case showed that there was a small deflection at the cable. For the wind case, there is asymmetry in the cable and large deformation occur. Anyhow, in the check of the capacity, all the requirements was fulfilled.

Keywords: Stress Ribbon, Timber, Roof Structures, Numerical Method, Load Combinations

CONTENTS

Preface

In this thesis a investigation of the Stress Ribbon concept has been carried out, where different load combinations affecting a cable shaped roof structure has been in central. The thesis has been performed at the Division of Structural Engineering, Department of Architecture and Civil Engineering, Chalmers University of Technology, Sweden, and in collaboration with WSP Sweden, business area WSP Construction Design. Examiner was Senior lecturer Joosef Leppänen and supervisors were Samuel Hofverberg and Alexander Sehlström at WSP Construction Design, Göteborg, Sweden.

The project is a continuation of Samuel Hofverbergs Master thesis "*Long-span tensile timber roof structures*" from 2016. The original idea of the Stress Ribbon concept in this context was generated by Professor Roberto Crocceti at the Division of Structural Engineering at Lund University, Sweden.

We are grateful for all valuable support and advice from our supervisors Samuel Hofverberg, Alexander Sehlström and our examiner Joosef Leppänen. We would also like to thank Fredrik Jonsson at WSP Construction Design for all advice with the FE-software ABAQUS.

Last but not least, we want to thank our opponents Carl Holmquist and Marcus Ahlström for their inputs and company during the work with this thesis.

Göteborg June 2017

David Gustafsson and Martin Ingvarsson

1 Introduction

1.1 Background

The environmental aspect is an important issue in the building industry nowadays. Therefore, the use of more environmental friendly material such as timber is desirable. An easy way to decrease the environmental impact is to reduce the amount of material in the structural system. When combining a low use of a material with a light-weight material, e.g. timber, the transportation time and cost are reduced which leads to reduced impact on the environment. Timber is also the only material that binds carbon dioxide through its photosynthesis process. This has led to an increasing interest to use timber in structures.

In order to decrease the number of structural elements and achieve a more open space, long-span structures are desirable. Common structural elements to implement in long span structures are e.g. truss system and arches made of either steel or timber. These structural systems are very efficient in order to achieve long-spans. The use of timber arches is a material efficient way to utilise the material where the timber receive compressive forces. Turning the arch upside-down into a cable shaped structure have been investigated. A few pedestrian bridges and buildings where the primary load bearing system is similar to the cable shaped timber element has been built. In 2016 the building Grandview Heights Aquatic Centre was completed. The primary load bearing system for this building is cable shaped timber elements where the longest span measures 65 m. Since timber has high capacity when it comes to tensile stresses, the cable shaped timber element is theoretically load- and material efficient compared to a straight simply supported beam (Johansson, 2016). The design and how to apply loads on the cable shaped structure are not covered in norms and standards.

The concept of transfer vertical load by a cable structure was studied by Hofverberg (2016), also called the stress-ribbon concept. Three different design solutions for the concept and designed the load bearing system for symmetric distributed load was developed. The results from his thesis indicate many advantages with the timber cable concept when it comes to material efficiency and environmental impact. However, asymmetrical load cases and how to analyse them were not included in this thesis.

1.2 Aim

The aim of this thesis is to investigate how asymmetrical loads affect the stress ribbon concept, which is defined as a cable shaped structure with inherent bending stiffness. The primary goal is to find a method how to analyse the stress ribbon structure for different types of load distributions. Therefore, a investigation of which loads that are important to take into consideration and how to apply them is carried out. Different analyse methods are compared to find a appropriate tool to perform a structural analysis of the stress ribbon structure.

1.3 Limitations

The stress ribbon concept is possible to apply on both bridge and roof structures. In this study the focus is to design the cable as a roof structure and relevant load combinations are investigated. How non-uniform loads affecting the timber cable structure is the main focus of the study. The design of the connection between the elements and the timber boundary truss system are of no concern. Neither the dynamic response on the structure is investigated.

The behaviour of the timber stress ribbon is the primary focus. Contribution from other structural elements in the roof structure, like plywood and corrugated steel, is not covered in this study. The span lengths that are investigated are 24 and 36 m. Design calculations and load combinations are performed with Eurocodes with the Swedish annex Boverket EKS in regard. The stress ribbon structure is designed for the local environmental parameters from Stockholm.

1.4 Method

To start with, a literature study of existing reference objects is carried out. This is investigated to get an increased understanding of the stress ribbon concept and to distinguish where it can be implemented. In order to design the structure for different load combinations, both analytical solution and computer calculation based on the finite element method, FE-models, are performed. The analytical solution is performed on three different load cases; symmetric load, asymmetric load and a central point load. The analytical solutions are thereafter compared with the the results from the FE-models in order to verify the model. Experimental reports and norms are investigated to find realistic load cases to apply on the stress ribbon structure. To find deformation and sectional forces for the realistic load cases two different software are compared and verified with analytical solutions. Following software are proposed to do the analysis of the structure, Karamba 1.2.2 which is a plug-in to Rhinoceros and the other option is ABAQUS/CAE 6.14-2. Furthermore, a case study is performed where the results from the analytical solution and the FE-models are compared and conclusions from the results are taken.

2 Previous work

There are several stress ribbon structures constructed around the globe. Some of these structures are presented and discussed in Section 2.1. Their structural behaviour and way of transferring loads are described. This is done to get a better understanding of the stress ribbon concept. Subsequently, a short summary of Hofverberg (2016) master thesis “*Long-span tensile timber roof structures*” is presented.

2.1 Reference projects

Several structures where the stress ribbon system is adopted is described in the following section. This is an investigation in order to get a better understanding and increasing knowledge of cable shaped structures. In the end of each reference study, a conclusion is drawn in order to gather information regarding the stress ribbon concept.

2.1.1 Grandview Heights Aquatic Centre

Grandview Heights Aquatic Centre, seen in Figure 2.1, is built in British Columbia in Canada and was completed in 2016. The building is designed by HCMA Architecture + Design and constructed by the firm Fast + Epp. There are several advantages with the system when it comes to material efficiency and reduced roof thickness which increases the free space inside the building. As can been seen in Figure 2.2 the load carrying roof structure is primary made of curved glulam beams which is suitable in humid environments for their resistance to warping due to moisture. The building is today the longest timber cable roof structure in the world (Naturally-Wood, 2016).

Figure 2.1: Exterior of Grandview Heights Aquatic Centre, (HCMA, 2016).

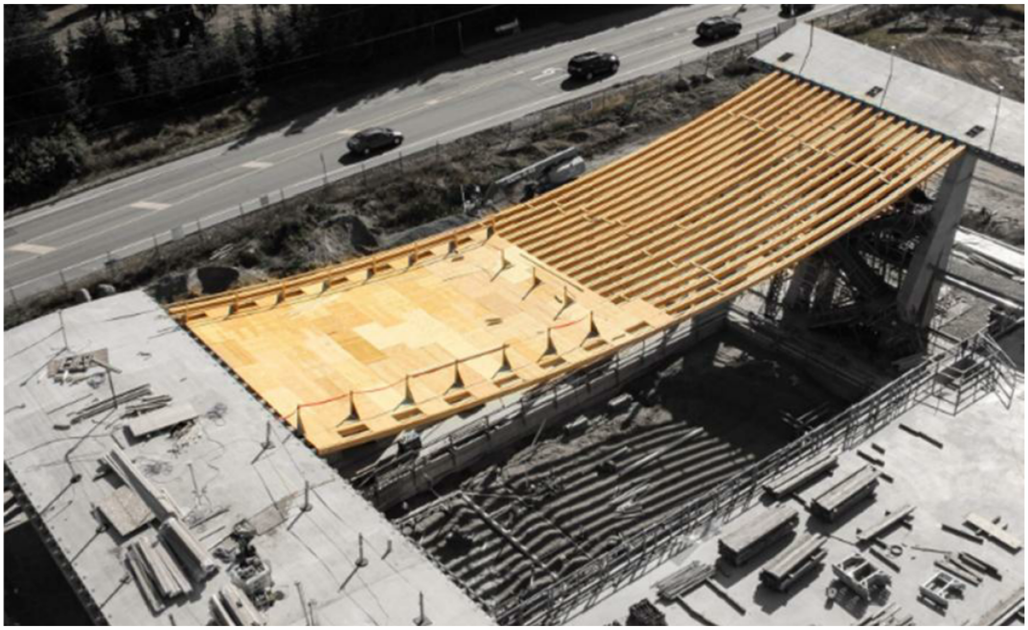

Figure 2.2: View from above during construction (HCMA, 2016).

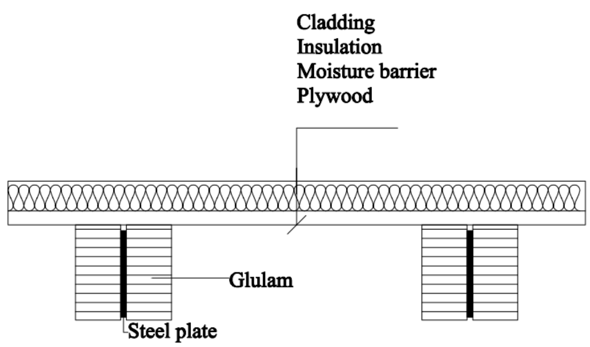

Figure 2.3: Section of the roof structure.

The curved glulam beams transfer the forces from the applied load to supporting concrete elements, which transfer the load to the foundation. The ribbon system is made of paired glulam beams, 130 x 220 mm^2, connected to each other by steel plates and with nailed plywood boards on top of the ribbons. A section of the roof structure can be seen in Figure 2.3. The distance between each pair is 700 mm. In Figure 2.4, a schematic section of the building is presented where the building has two spans with 65 respectively 45 m. In order to joint the elements, the glulam beams have been produced in parts of different length and then been connected to each other on site. The stiffness of the members give the building stability against wind uplift, which makes the timber choice suitable compared to a system with steel cables without bending stiffness. The maximum designed deflection for the roof under the most severe load case is 200 mm as this is the limited value for the used wall slip joint detail (Naturally-Wood, 2016).

The concrete columns has a design, where the columns only work in compression on the left side and in compression and tension on the right side, as can been seen in Figure 2.4. In the middle of the building the two columns take compression forces and transfer it further to the foundation that also needs to resist rotational stiffness. The roof is constructed with a certain slope, where the corners have different height, in order to achieve drainage.

The design of the timber ribbon system shows that the desirable long span length can be achieved with this kind of structure. The paired ribbons with the inserted steel plate in between simplify the connection to the concrete support. The slope of the roof is also preferable since drainage is achieved.

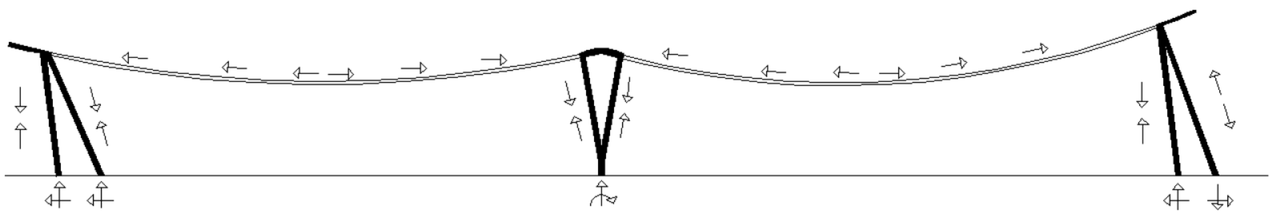

Figure 2.4: Illustration of Grandview Heights Aquatic Center, adopted from HCMA (2016).

2.1.2 Gessental Bridge

The Gessental Bridge is located in Ronneburg in Germany. It was completed in 2006 and designed by Büro für Ingeniur-Architektur and is one of the longest timber bridges in the world (Jeska, 2014). The total length is 225 m including three spans, 52.5, 55 and 52.5 m respectively, see Figure 2.5. The maximum sag in mid-span is 2.3 m. The primary tensile structure consists of 50 cm high glulam beams. In Figure 2.6, sections of the bridge and the connection between different parts are displayed. In order to prevent large deformation along the walkway, additional glulam beams were added which increased in height towards the middle of the span, see Figure 2.6. This also reduces the slope of the bridge. To transfer the tensile forces to the abutment the middle supports allow the bridge to move free in the length direction of the bridge, but is fixed in the transverse direction (Jeska, 2014).

(a)

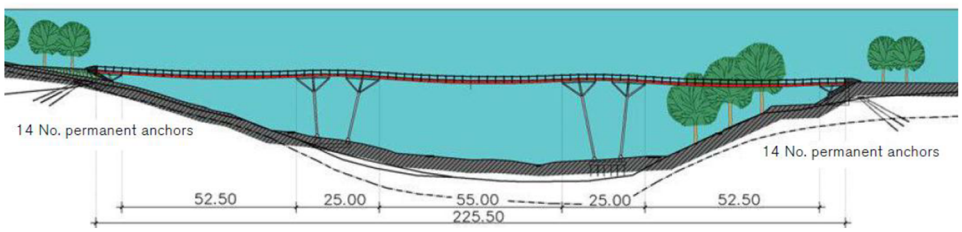

(b)

Figure 2.5: a) View from beside the bridge, b) Elevation of the bridge, (Jeska, 2014).

The stress ribbon bridge consists of nine prefabricated segments, which were assembled together at the building site. In order to connect each segment to each other, steel plates were installed at the end of each segment. Over 400 steel dowels were used to connect the plates to the glulam beams. During production, temporary supports were used in order to connect the segments, and when the temporary supports were removed, the bridge achieved its final shape. Stress ribbon bridges loaded primarily in tension, usually are made of either reinforced concrete or steel. The use of timber in this structure instead of reinforced concrete reduces the self-weight which in turn lead to smaller tensile forces. Consequently, the cost for heavy concrete abutments were decreased (Jeska, 2014). This indicates that the choice of timber is suitable for this kind of projects.

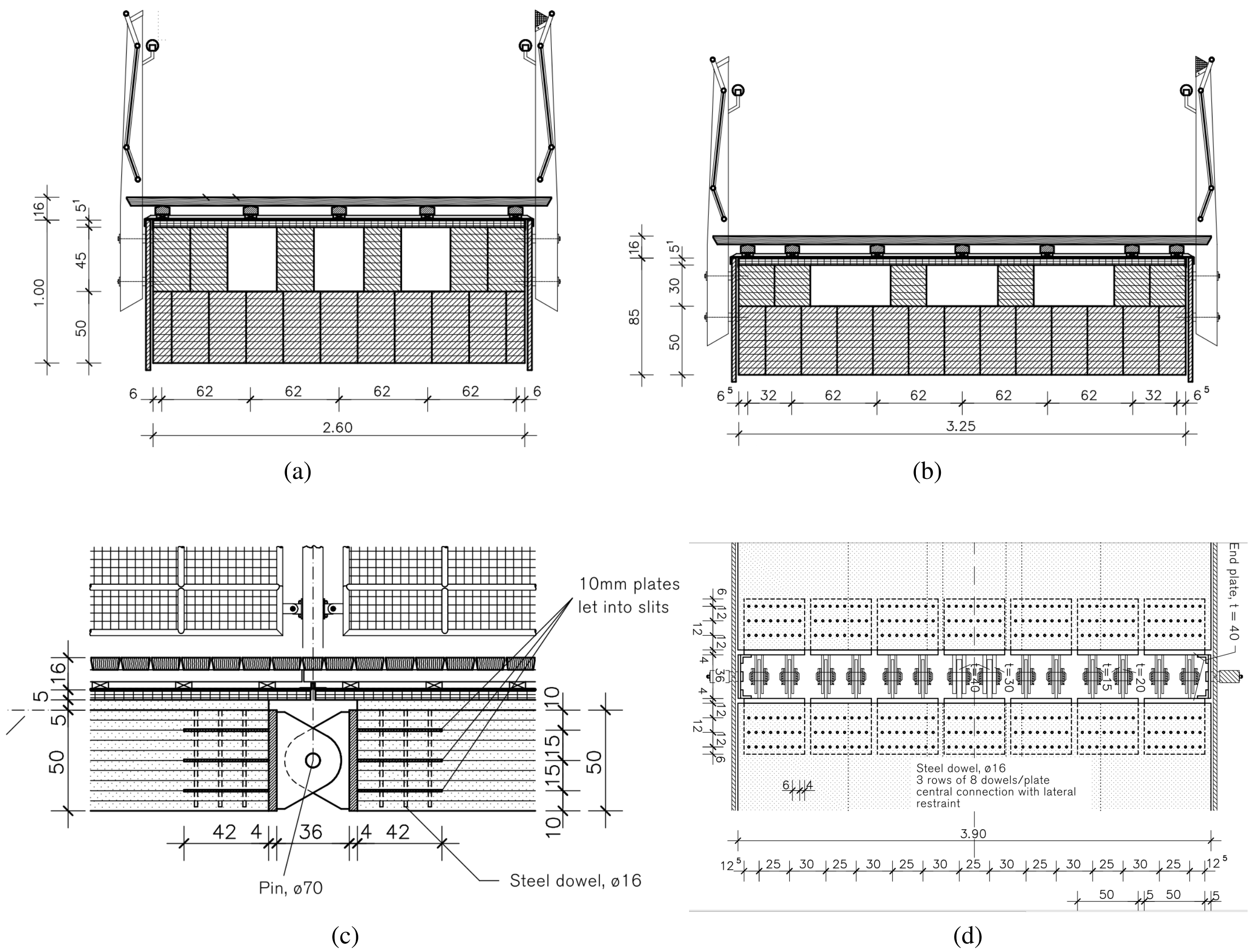

Figure 2.6: Section of the bridge, a) section at the mid span, b) section at the supports, c) connection of section, d) connection of segments, view from above, (Jeska, 2014).

2.1.3 New Braga Municipal Stadium

The New Braga Municipal Stadium, seen in Figure 2.7, was built as a part of the preparations to the Euro Championship in Portugal, completed in 2003. The architect of the stadium was Eduardo Souto de Moura. The concept of the stadium is to stretch cables between the two grandstands in order to avoid using columns for supporting the roof. The stadium has brought attention for its design and has been considered a masterpiece according to Magalhaes, Caetano, and Cunha (2007).

Figure 2.7: View of the Braga Stadium, (Magalhaes, Caetano, & Cunha, 2007).

The roof is suspended by steel cables, with limited bending stiffness. In order to get stability of the roof, 245 mm thick concrete elements are connected on top of the cables, see Figure 2.8. The space between the two stands is 202 m. The concrete elements have a length of 57.3 m on each side, and the open span over the pitch measures 88.4 m. The east stand is built of sixteen concrete elements, each 50 m high. They are formed in a certain shape as seen in Figure 2.8, to compensate the tensile forces from the roof and minimise the moment at the foundation (afaconsult, 2005). The west stand is constructed at the side of the mountain and the tensile cables are directly anchored into the rock massif (Magalhaes et al., 2007). On the top of the both stands, a stiff beam is placed in order to transfer the tensile forces from the roof to the wall elements.

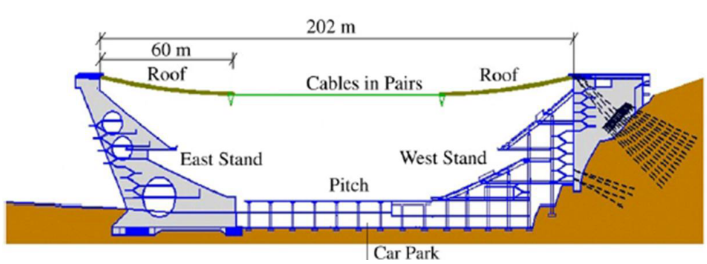

Figure 2.8: Section of the stadium illustrating how the structure is anchored to the ground, (Magalhaes, Caetano, & Cunha, 2007).

The desire in this project was to exclude columns supporting the roof structure, in order to achieve a open space at the stands. The primary load-bearing system consist of cables with limited bending stiffness but additional distributed concrete elements on top of the cables on each side in order to provide stiffness to the roof structure. The efficiency of transfering loads and excluding of columns make the development of the stress ribbon concept of interest.

2.1.4 Nagano Olympic Memorial Arena

The Nagano Olympic Memorial Arena was built for the Olympic winter games in 1998, an illustration of the cable shaped structure can be seen in Figure 2.9. It is one of the largest speed skating arenas with room for 10 000 visitors. It has a free spacing of 80 x 216 m.

Generally hanging roof structures easily deform due to the uplifting forces caused by wind loads. The uplift force can be resisted by pretension cables, which is further explained in Chapter 3 and can be seen in Figure 3.3. However, in this case the cable itself is provided with bending stiffness and is therefore able to resist the uplifting force.

Figure 2.9: The Olympic arena in Nagano, (Ban, Motohashi, Yoshida, & Tsubota, 1999).

The hanging roof consists of 15 roof panels, where each of the panel consists of a composite element, see Figure 2.10. The span length of the roof is 80 m and each segment has a width of 18 m. The sag of each segment is 5 m. The roof consists of paired glulam beams, with a dimension of 300 x 125 mm^2, and a steel plate in between, 200 x 12 mm^2. The plate is connected to the glulam beams with steel bolts with a spacing of 600 mm in between. The glulam beams together with the steel plates give transverse stability. To resist the horizontal wind loads, plywood panels are nailed on top of the beams to increase the transversal stiffness, (Ban, Motohashi, Yoshida, & Tsubota, 1999).

The wall elements are connected to the roof panels and transfer the load further to the foundation. How the forces are acting on the structure can be seen in Figure 2.11. The walls consist of posts and stays, where the post resists compression and the stay resists tension forces. The walls are pin connected to the roof elements. Counterweights, made of reinforced concrete, are added to resist the tensile forces from the stays, see Figure 2.11 (Ban et al., 1999).

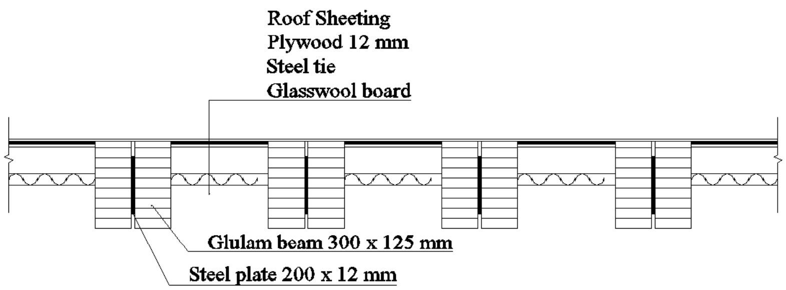

Figure 2.10: Section of the composite roof.

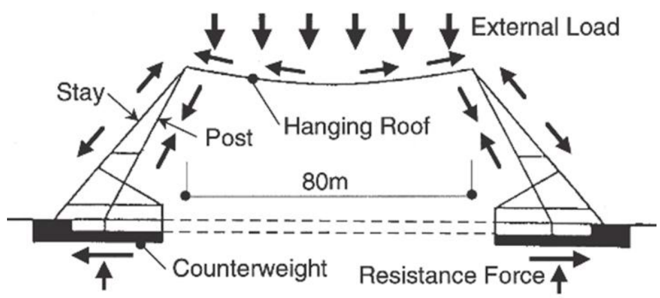

Figure 2.11: Section of the building explaining how forces are transferred (Ban, Motohashi, Yoshida, & Tsubota, 1999)

.

The load carrying concept of this building is similar to Grandview Heights Aquatic Centre. The long span length with the low construction height of the roof structure enables the desired open space in the building. The contribution from the steel plate in the roof structure is not further described in Ban et al. (1999) and therefore no conclusions whether what kind of impact the timber cable has on the load bearing system can be analysed.

2.1.5 Essing Timber Bridge

The 192 m long timber bridge designed for pedestrians was opened in 1992 and is loacated in Essing, Germany, see Figure 2.12. The timber bridge spans over the Rhein-Main-Donau Canal. The architect of the bridge is Richard J. Dietrich and the structural engineer is Heinz Brünninghoff.

(a) side-view of the bridge.

(b) view at the walkway.

Figure 2.12: Illustrations of the bridge (Brünninghoff, 1993).

The bridge is designed as a hanging cable, which makes it possible to transfer vertical loads through axial tension to the supports. The system consists of nine glulam beams, 220 x 650 mm^2, arranged together in groups of three, see Figure 2.13. This relatively low cross section compared to the span length was chosen to minimize the bending stiffness in the structure and force it to act in tension. The truss supports are also made of glulam, and transfer the load further to the concrete abutments. To achieve lateral stability steel rods is installed as cross bracing in the supports to transfer horizontal loads into each foundation. Underneath the walkway, a crosswise timber bracing system is installed to give the bridge stiffness against lateral loads. In order to achieve a long service life, the bridge is coated with a waterproof sheet of titanium zinc (Brünninghoff, 1993).

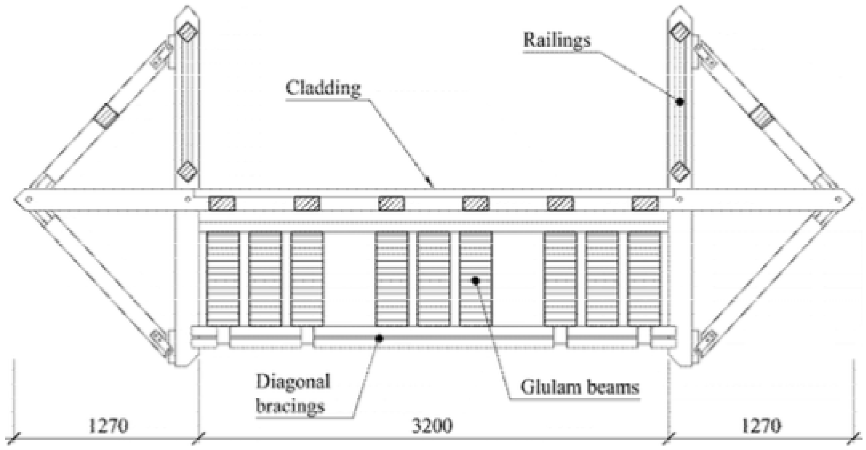

Figure 2.13: Section of the timber bridge (Hofverberg, 2016).

The bridge consists of three spans, where the main span is 73 m long. The sag of each span is designed differently in order to receive the same tension force. The maximum designed tensile force is 4000 kN. The aim to have the structure working 90% in tension and 10 % in bending was achieved. The glulam beams are prefabricated in lengths of 40-45 m. The connection of each glulam element is achieved by finger jointing at site (Brünninghoff, 1993).

This project show that the use of timber in cable shaped structures is applicable. The efficiency of transfer tensile forces in this structure indicate that the use of timber in tensile structures have several advantages.

2.2 Design proposal of the stress-ribbon concept

The study performed by Hofverberg (2016) present the stress-ribbon concept with the implementation of timber. A considered span length of 24, 36 and 48 m of the cable was investigated. A preliminary design of the structure, with three different design proposals was evaluated. Where an analytical study of how symmetric load distribution affect the roof structure was performed. An investigation of how non-uniform loads affect the roof structure was proposed by Hofverberg (2016), in order to design the roof for realistic load cases. An illustration of the structure can be seen in Figure 2.14.

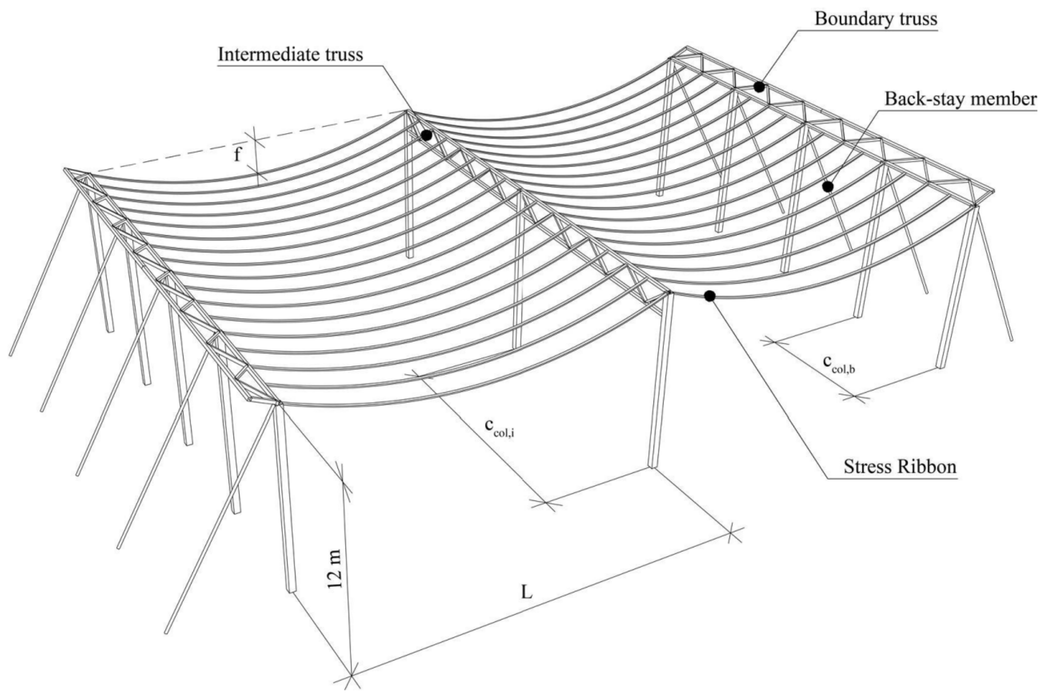

Figure 2.14: View of the structural system.

In order to design the roof structure, three different proposals were presented. The following proposals are further explained below.

The first proposal is based on a sparse system of timber ribbons, see Figure 2.15 (a). The geometry of the ribbons are rectangular and with a distance of 8 m between each member. In this proposal each ribbon is connected to one column at the edges, which transfer the forces further to the foundation. In the middle of the building the spacing is 16 m between the columns and a timber truss system is assembled in order to connect the ribbons. This system requires large dimensions of each ribbon since large loads are subjected to each member.

The second proposal is designed with a spacing of 0.8 m between the ribbons, see Figure 2.15 (b). As in proposal 1, the ribbons are rectangular. The short distance between each member gives more material efficiency compared to proposal 1. This alternative also has the advantage if one member would lose its load-bearing capacity, the systems itself would not been significant affected. The disadvantage of the system is that an extra structural element has to be added in order to transfer the forces from the ribbons. The added boundary truss needs to resist both horizontal and vertical forces. The assemblage of the boundary truss also leads to more material usage and more complicated production of the system.

The third system consists of LVL panels, which forms into a continuously surface, see Figure 2.15 (c). As in proposal 2, the system needs to be connected to an added boundary truss in order to transfer horizontal and vertical loads to the column. Advantage of this system is that the panels can be utilised in resist the horizontal force by diaphragm action. The number of elements is therefore decreased.

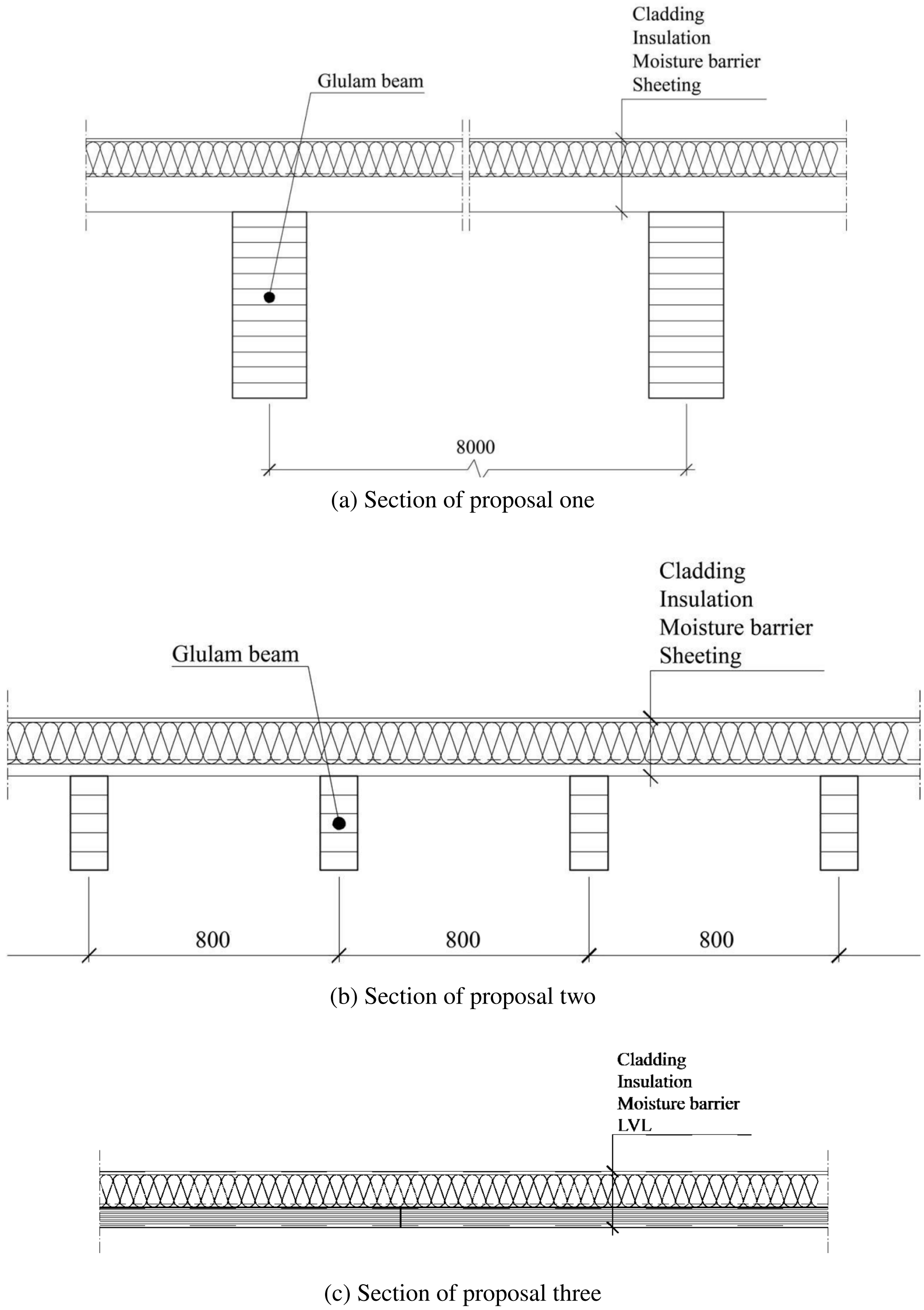

Figure 2.15: Ilustrations of the different design proposals investigated by Hofverberg (2016).

A comparison of the material usage of the three different proposals was performed according to Hofverberg (2016). The most material efficient proposal was the second one. A calculation according to ultimate limit state was performed for proposal two and three and the design requirements was fulfilled. Henceforth, the basic design of proposal two is used in this thesis for further analysis.

3 Stress Ribbon concept

This chapter covers a brief introduction to cable shaped construction systems. How the structural system is working, different possibilities to transfer loads to the foundation and basic ways to get stability are discussed. Furthermore, a short description of curved glulam beams is presented.

3.1 Cable shaped structures

The technique of building roofs with tension members is very old. Thousands years of history show that people have protected themselves from the surrounding climate with tension structures e.g. tents (Krishna, 2015). The first modern cable shaped roof structure, completed in 1953, was the the North Carolina State Fair Arena in Raleigh, USA (Buchholdt, 1999). This way of transfer axial tension forces made it possible to span over long distances with a relatively low cost. In Figure 3.1 the stress distribution for a member in tension and bending is shown. This figure indicates that members in tension have a higher utilisation ratio compared to one subjected to bending.

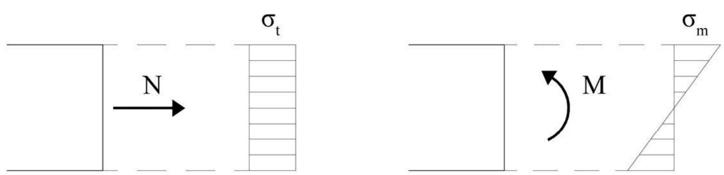

Figure 3.1: Stress distribution for a member in tension and bending

The possibility to reduce the amount of columns is a great advantages with cables structures. Therefore, cable structures are suitable in buildings as stadiums, sports halls, swimming pools, hangars and warehouses where long spans are required. According to Buchholdt (1999) cable structures can be divided into four different categories;

1. Simply supported cables
2. Pretensioned cable beams
3. Pretensioned cable nets
4. Pretensioned cable grids

The focus of this thesis is on alternative 1. Simply supported cables but with bending stiffness. In this alternative the cable is spanning between two supports. The attachment between the cable element and support is a hinged connection, in that sense no bending moment is transferred from the cable to the supporting structure. However, the supporting structures needs to handle the high tension forces that are developed in the cable. This can be achieved by different solutions, as it is possible to recognize in the reference objects presented in Section 2.1. For example the supports at Grandview Heights Aquatic Centre are composed of inclined concrete elements working in compression, see Figure 3.2 (b). The heavy concrete elements, in comparison to the cable system, create a rigid support structure. The east stands at Braga Municipal Stadium is made of inclined concrete elements. The inclination create an eccentricity of the gravity centre to compensate for the tensile forces, this can be seen as a combination of option (b) and (c) in Figure 3.2. The west stand at Braga Stadium is directly anchored in the ground by tendons. This can be compared to back-stay cables in a cable-stayed bridge. The supports at Nagano Olympic Memorial Arena is composed of a post and stay system, similar to Figure 3.2 (a).

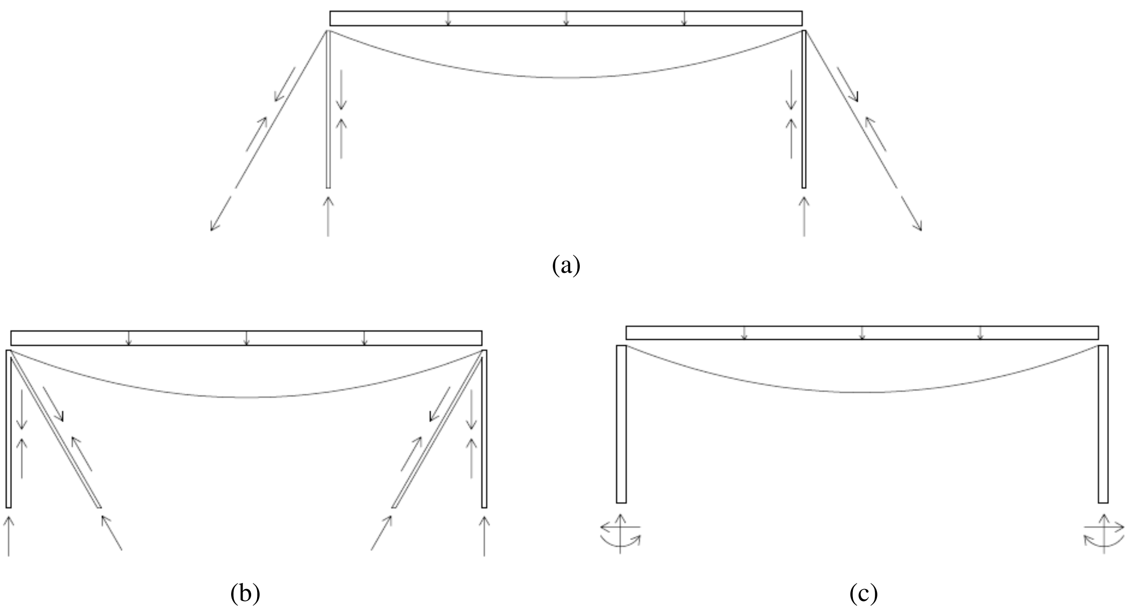

Figure 3.2: Schematic support configurations for a cable system.

In the first option (a) the tension forces are transferred to the ground by the inclined tension members while the vertical struts handle the vertical forces. The forces in the inclined members increase with the slope. With a steep slope the requirements of the foundation increases. The foundation for the inclined members does not only have to withstand the lateral force but also an uplift effect. In option (b) the horizontal forces are resisted by the inclined compression members. As they are in compression a risk of buckling exists. The foundation needs to handle both horizontal and vertical forces.

The last presented option (c) is composed of moment resistant columns. They have the same behaviour as cantilever beams and need to handle all horizontal force and induced bending moment at the ground level in the foundation. This option is suitable when loads are rather low and the span is short (Schodek & Bechthold, 2014).

When the sag in a cable increases, the internal axial forces decrease. On the other hand, the height of the structure needs to be increased which causes longer elements and the risk of buckling in compressed members increases.

To get stability in a cable roof structure, several different alternatives are provided. A common way is to add self-weight to the cable roof, it can be achieved by using concrete elements as roof cladding, an example of this is Dulles International Airport outside of Washington D.C. An alternative can also be to provide the cable with bending stiffness in itself. This alternative is used in e.g. Grandview Heights Aquatic Centre described in Section 2.1.1 and Nagano Olympic Memorial Arena described in Section 2.1.4, where the cable shaped roof is composed of curved glulam beams. Other examples to achieve stiffness in the system is to add a tension cable with reverse curvature and connect it to the load-bearing cable with compression (struts) or/and tension (ties) members, see Figure 3.3. In alternative (a) the pretension force is created by struts while it is the opposite for alternative (b) where the pretension force in the load-bearing cable is generated by ties. Alternative (c) is a combination of (a) and (b). Alternative (d) give a similar behaviour to (b) but with a different configuration of the tie members.

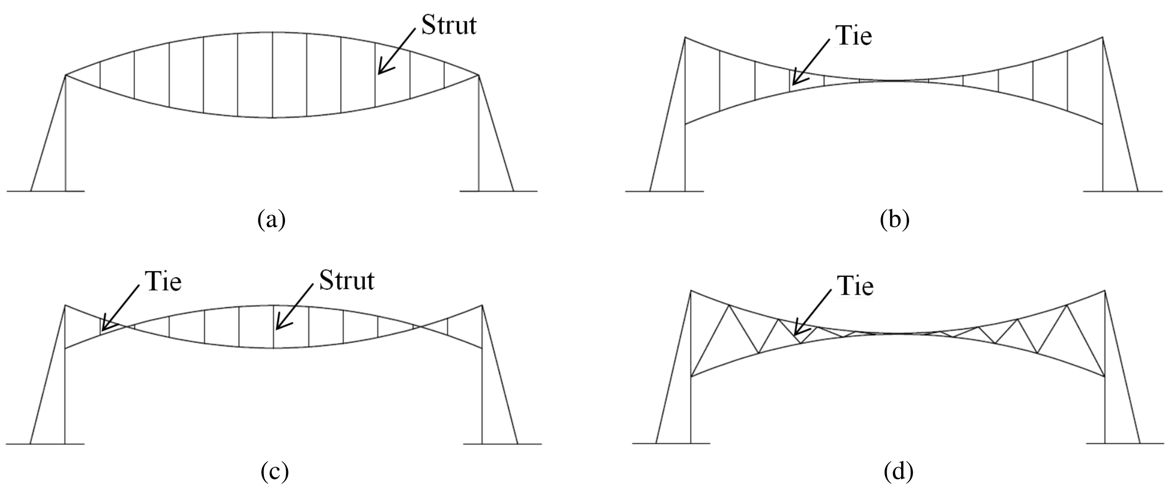

Figure 3.3: Four different configurations to use pretension cables to add stiffness to the system, adopted from Buchholdt (1999).

3.2 Curved glulam beams

Glulam beams are possible to manufacture in various shapes, such as curved, pitched and tapered (Linville, 2012). During production of curved glulam beams laminates are bent and glued together to get their final curved shape. The glue locks the timber laminates together and makes them retain their curvature (Jeska, Pascha, & Hascher, 2014). When manufacturing curved beams residual stresses are introduced, which reduce the bending capacity of the beam. This aspect is in SS-EN 1995-1-1 (CEN, 2009) handled with a reduction factor k_r which consider loss of strength during bending of the laminates. Limits of the minimum radius of a curved glulam beam to minimize the induced stresses are recommended. If the limits are exceeded a risk of irreparable damage or breaking occur (Linville, 2012). The limits depend on the thickness of each laminate and the material properties of the timber. A smaller thickness of the laminate makes it easier to bend and consequently reach a shorter radius.

Stresses perpendicular to the grain are introduced when a curved timber member is subjected to bending moments. When a curved beam in a stress ribbon system is subjected with a gravity load, the radius has a tendency to get shorter and compressive stresses perpendicular to the grain is induced. Obviously, the opposite will occur when the structure is subjected with an uplift force i.e. tension stresses are induced perpendicular to the grain, see Figure 3.4. Henceforth, these effects are not considered, as the primary action of the catenary roof structure is axial tension.

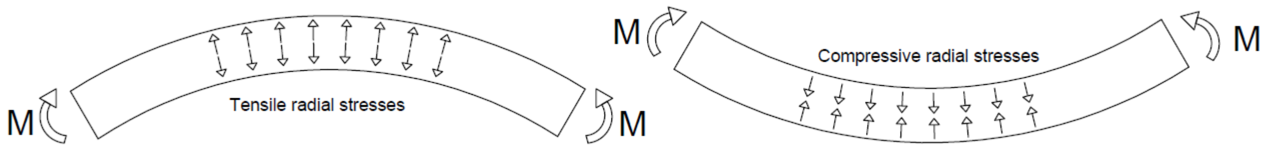

Figure 3.4: Radial stresses on a curved beam, adopted from Reza Haghani[1]

[1]Lecture 8 in Timber Structures 2017 at Chalmers University of Technology

4 Analytical solutions

In this chapter, analytical solutions for the cable behaviour with inherent bending stiffness are presented. These analytical solutions will be used and compared with the FE-model. A third analytical solution will also be used later, where the cable is subjected to a uniform distributed load, this solution is presented in Hofverberg (2016).

4.1 Asymmetric imposed load

Deflection for a cable subjected to an asymmetric load, in this case load in half of the span, see Figure 4.1, can be expressed as eq. (4.1) and (4.2). Eq. (4.1) describes deflection w_1 when the span is subjected to imposed load and eq. (4.2) describes the deflection w_2 when only self-weight is applied.

The following equations for a cable with bending stiffness subjected to an asymmetric load as seen in Figure 4.1 are described by Marti (2013).

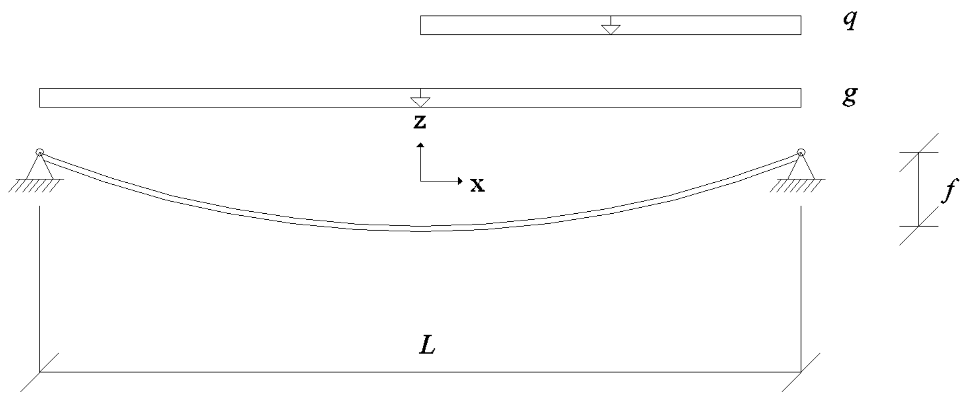

Figure 4.1: The cable subjected to asymmetric load.

- w - Deflection [m]
- f - initial sag [m]
- q - Imposed load [kN/m]
- g - Self-weight [kN/m]
- H - Horizontal tension due to permanent load g [N]
- ΔH - Change in horizontal tension due to imposed load q [N]

$$w_1 = c_1 + c_2 x + c_3 \cosh(\lambda x) + c_4 \sinh(\lambda x) - \frac{q - g\frac{\Delta H}{H}}{2(H + \Delta H)} x^2 \tag{4.1}$$

$$w_2 = c_5 + c_6 x + c_7 \cosh(\lambda x) + c_8 \sinh(\lambda x) - \frac{g\frac{\Delta H}{H}}{2(H + \Delta H)} x^2 \tag{4.2}$$

where w_1 describes the deflection in the part of the span with imposed load, while w_2 is the deflection in the part of the span without imposed load. With the following boundary conditions, where L is the total horizontal length of the cable and origo is located in the middle between the two supports, thus $x = L/2$ and $x = -L/2$ are the support positions.

$$w_1\Big(-\frac{L}{2}\Big) = w_1''\Big(-\frac{L}{2}\Big) = w_2\Big(-\frac{L}{2}\Big) = w_2''\Big(-\frac{L}{2}\Big) = 0 \tag{4.3}$$

and the continuity conditions,

$$\begin{gathered} w_1(0) = w_2(0) \\ w_2'(0) = w_2'(0) \\ w_2''(0) = w_2''(0) \\ w_2'''(0) = w_2'''(0) \end{gathered}$$

gives the following constants which will be input in the eq. 4.1 and 4.2, in order to determine the deflection.

$$c_1 = \frac{\Big(q - g\frac{\Delta H}{H}\Big)\Big(\frac{L^2}{8} - \frac{2}{\lambda^2}\Big) - \frac{L^2}{8} g \frac{\Delta H}{H}}{2(H + \Delta H)} \tag{4.4}$$

$$c_2 = c_6 = \frac{-qL}{8(H + \Delta H)} \tag{4.5}$$

$$c_3 = \frac{-q\Big(cosh\Big(\frac{\lambda L}{2}\Big) + 1\Big) - 2g\frac{\Delta H}{H}}{2(H + \Delta H)\lambda^2 cosh\Big(\frac{\lambda L}{2}\Big)} \tag{4.6}$$

$$c_4 = c_8 = \frac{qcosh\Big(\frac{\lambda L}{2}\Big) - 1}{2\Big(H + \Delta H\Big)\lambda^2 sinh\Big(\frac{\lambda L}{2}\Big)} \tag{4.7}$$

$$c_5 = \frac{\left(q - 2g\frac{\Delta H}{H}\right)\frac{L^2}{8} + \frac{2}{\lambda^2}g\frac{\Delta H}{H}}{2(H + \Delta H}) \tag{4.8}$$

$$c_7 = \frac{-q\left(cosh\left(\frac{\lambda L}{2}\right) - 1\right) - 2g\frac{\Delta H}{H}}{2(H + \Delta H)\lambda^2 \cosh\left(\frac{\lambda L}{2}\right)} \tag{4.9}$$

Eq. (4.1) and (4.2) inserted in

$$\Delta H = \frac{8fEA}{L^3}\int_0^L w dx \tag{4.10}$$

gives the change of horizontal tension force ΔH as

$$\Delta H = \frac{\left(q - 2g\frac{\Delta H}{H}\right)fEA}{(H + \Delta H)}\left[\frac{L}{3} - \frac{4}{(\lambda L)^2} + \frac{8tanh\left(\frac{\lambda L}{2}\right)}{(\lambda L)^3}\right]. \tag{4.11}$$

According to beam theory, the bending moment is expressed as

$$M = EIw'' \tag{4.12}$$

Where E and I are Young's modulus and moment of inertia respectively and w'' is the curvature. By differentiating eq. (4.1) and (4.2) twice and insert in eq. (4.3) the bending moments in the structure can be calculated, see Appendix A1.4.

4.2 Central point load

In this section, a central point load is assumed to act on the cable structure. An analytical solution described by Marti (2013) is presented with consideration to bending stiffness.

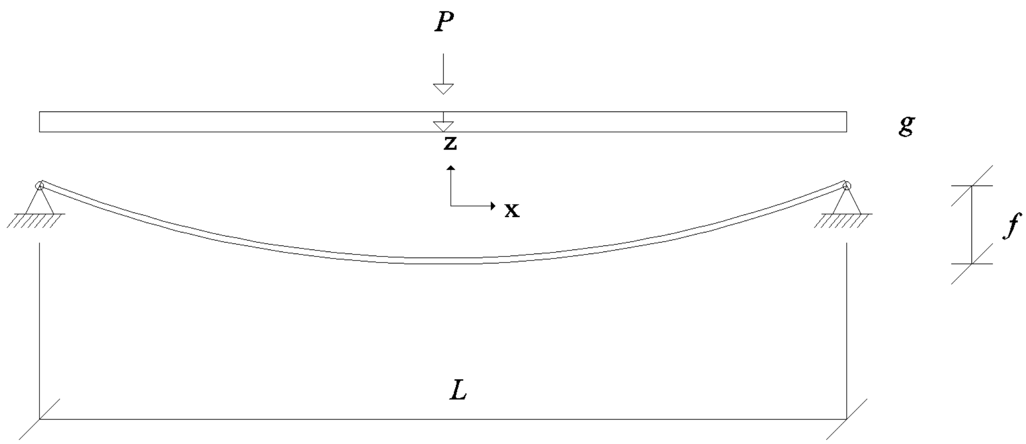

Figure 4.2: Structural scheme of a point load applied at midspan.

The deflection can be calculated as

$$w_1 = c_1 + c_2 x + c_3 \cosh(\lambda x) + c_4 \sinh(\lambda x) - \frac{q - g\frac{\Delta H}{H}}{2(H + \Delta H)} x^2 + w_{part} \tag{4.13}$$

with the particular solution,

$$w_{part} = \frac{\Delta H g x^2}{2H(H + \Delta H)} \tag{4.14}$$

the following boundary conditions

$$w\left(\frac{L}{2}\right) = w''\left(\frac{L}{2}\right) = w'(0) = 0$$

and the continuity conditions

$$-EIw'''(0) = -\frac{q}{2} \tag{4.15}$$

gives the following constants

$$c_1 = \frac{\frac{qL}{4} - g\frac{\Delta H}{H}\left(\frac{L^2}{8} - \frac{1}{\lambda^2}\right)}{2(H + \Delta H)} \tag{4.16}$$

$$c_2 = \frac{-q}{2(H + \delta H)} \tag{4.17}$$

$$c_3 = \frac{\frac{q}{2\lambda} sinh\left(\frac{\lambda L}{2}\right) + \frac{g}{\lambda^2}\frac{\Delta H}{H}}{(H + \Delta H) cosh\left(\frac{\lambda l}{2}\right)} \tag{4.18}$$

$$c_4 = \frac{q}{2\lambda(H + \Delta H)} \tag{4.19}$$

These constants inserted in eq. (4.13) together with eq. (4.10) for deflection gives the change of horizontal tension force ΔH as

$$\Delta H = \frac{16fEA}{(H + \Delta H)}\left[\frac{q}{L}\left[\frac{1}{16} - \frac{1}{2(\lambda L)^2} + \frac{1}{2(\lambda L)^2 cosh\left(\frac{\lambda l}{2}\right)}\right] - g\frac{\Delta H}{H}\left[\frac{1}{24} - \frac{1}{2(\lambda L)^2} + \frac{tanh\left(\frac{\lambda L}{2}\right)}{(\lambda L)^3}\right]\right]. \tag{4.20}$$

5 Numerical solutions

The basics of how to solve finite element problems and a description of geometrical non-linearity are presented in this chapter. This is done in order to get an understanding of how the system can be analysed with help of computer programs. To analyse the stress ribbon structure two FE-software programs are chosen to be investigated. The programs used for modelling and analysing are ABAQUS/CAE 6.14-2 and Karamba 1.2.2.

5.1 The basics of the finite element method

All kinds of engineering mechanics are modelled by differential equations, and usually the problems are advanced to handle and difficult to solve analytically. The finite element method is a numerical approach where the problems are solved by differential equations in an approximate way.

The region which the differential equations describes can be one-, two- or three-dimensional. The basics of the finite element method feature that instead of approximate a whole region directly, the region is divided into smaller areas and then the approximation over the whole region can be analysed. In many cases the differential variation is non-linear and therefore it is useful to approximate each area into linear behaviour, so called finite element mesh.

When the region has been divided into finite elements, each element can be analysed separately. When all elements are determined, these can be linked together in order to form the whole region, which will be the approximate solution. The approximation is usually polynomial and can be described with some kind of interpolation over each element where the start and end value is known. The start and end points are called nodal points. In Figure 5.1, an illustration of a non-linear function over a certain region is presented. Non-linear problems can be to hard to solve analytically therefore FEM can be a tool to solve these problems. The finite element method handles these non-linearity problems by using approximate regions, as mentioned in the beginning of this section (Ottosen & Petersson, 1992). The approximate solution for the non-linear function can be visualised in 5.2 (a), and the division of the region into smaller elements can be seen in 5.2 (b)

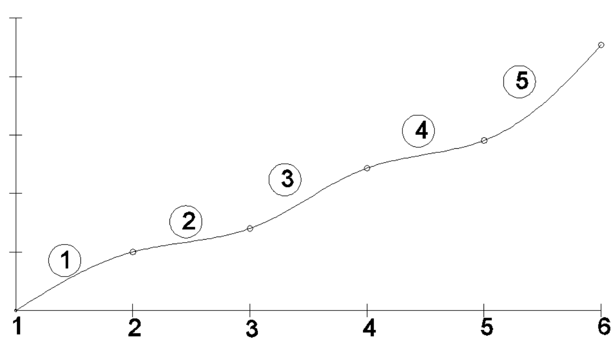

Figure 5.1: Example of non-linear behaviour

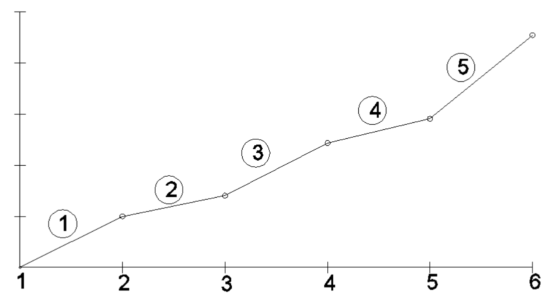

(a)

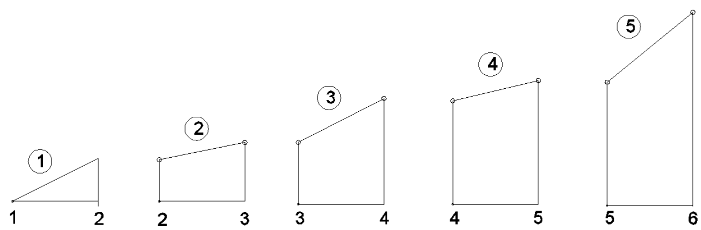

(b)

Figure 5.2: a) Approximation of the graph in Figure 5.1, b) Division of the region into smaller areas.

5.2 Geometrical non-linearity

Due to large deformations, a stress ribbon structure needs to take geometrical non-linearity into account in the analysis stage. This section describe the basics of geometrical non-linearity with a simply supported beam as an example.

An illustration of a beam subjected with a point load, acting at the middle of the beam, shows how the deflection is affected by a tensile and a compressive axial force, Q, see Figure 5.4. When Q is tensioning the beam, the deflection decreases, while when Q is compressing the beam, the deflection increases. The force Q affects the stiffness of the beam, where the tensile and the compressive force increases respectively decreases the stiffness of it. In the linear case, Q acts on the initially straight beam and does not affect the deflection of it. With a more accurate model, where the equilibrium conditions are stated in a deformed shape, the phenomenon can be seen. The calculation procedure is non-linear and an iterative solution has to be performed. This kind of calculation procedure where the equilibrium conditions for the structure is stated in an deformed shape, is called geometric non-linear (Dahlblom & Olsson, 2010).

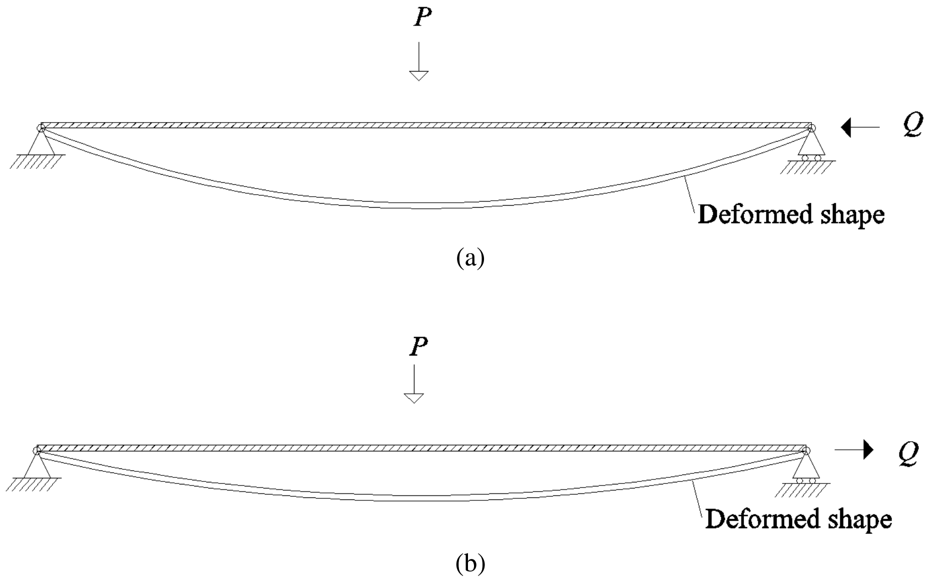

Figure 5.3: The deformation of a simply supported beam caused by a point load and the affect of, a) a compressive horizontal force, b) a tensile horizontal force.

The FE-model of the stress ribbon structure consists of beam elements in this thesis. Six degrees of freedom are needed to describe a beam element. Q_x describes the internal normal force for the deformed element. The beam element on matrix formulation with geometrical non-linearity in regard is expressed as

$$\bar{\mathbf{K}}^e \bar{\mathbf{a}}^e = \bar{\mathbf{f}}^e \tag{5.1}$$

where the matrix of the element stiffness $\bar{\mathbf{K}}^e$ consists of two parts, $\bar{\mathbf{K}}_0^e$ that is depending on the initial stiffness of the beam and $\bar{\mathbf{K}}_\sigma^e$ that is describing the axial force's Q_x impact on the stiffness (Dahlblom & Olsson, 2010).

A cable shaped structure subjected to load has a non-linear behaviour along its length. This can be called geometric non-linearity and is important to distinguish. A cable subjected to load has to follow its funicular curve and experience geometric adjustments, especially when the load is asymmetric. Unaffected by if the material itself has linear or non-linear stress-strain curves, there is geometric non-linearity in the cable. In Figure 5.4 an illustration of how an asymmetric load affects the shape of the cable is visualised (Krishna, 2015).

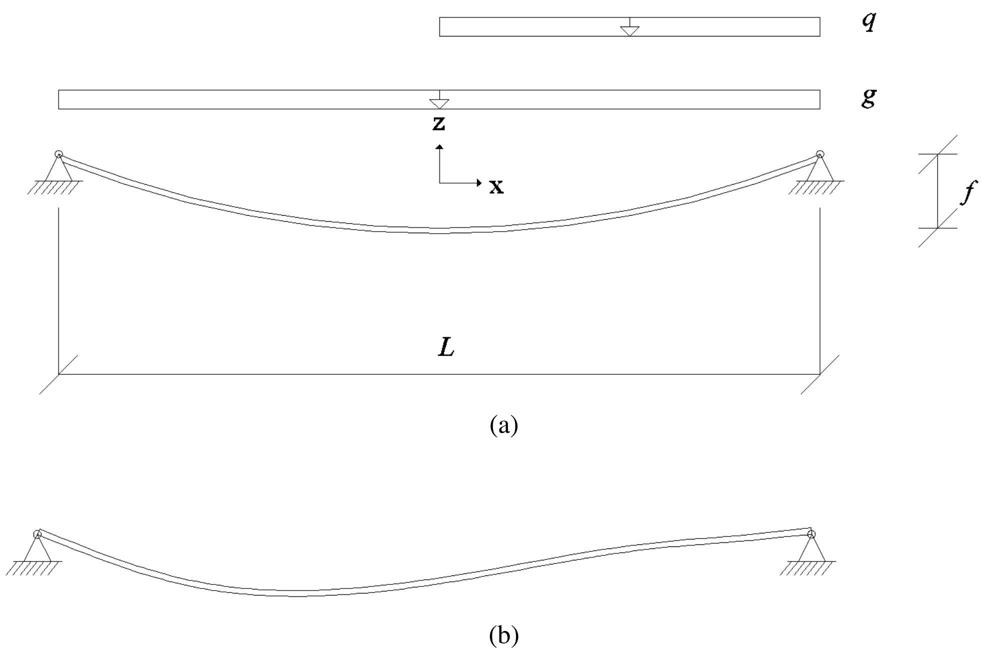

Figure 5.4: Illustration of the deformed shape of a cable subjected to asymmetric load.

In order to analysis a cable roof structure, it can be treated as a continuous membrane, or as a discrete system. If the structure is a discrete system, the method of analysis has to lend itself to the solution of stiffness or flexibility matrices set up for the structure. The using of iterative solution will be essential for this kind of non-linear problems. The Newton-Raphson method is a suitable method in order to handle the non-linear problem. Another proposed alternative solution to an stiffness or flexibility matrix analysis is the principle of minimization of total potential energy. This procedure uses conjugate gradients with step-length control and the Newton-Raphson procedure, and has improved results (Krishna, 2015).

5.3 FE-programs

5.3.1 Karamba

Karamba is a parametrical structural design toolkit which is a plug-in to Grasshopper3d. Grasshopper, in turn is a tool which describes geometries in Rhinoceros (CAD program) with a visual way of programming. Grasshopper uses boxes with commands or data which are linked together by lines. The data is transferred from left to right.

Karamba uses the same interface and logical state of mind as Grasshopper but provides the model with information about the structural response and enables performing structural analysis. Beam, shell and truss elements can be analysed by the Karamba. The program forms an easy-to-use and powerful tool for a structural engineer that in a fast and visual way gives the response of the structure (Preisinger & Heimrath, 2014).

Modelling in Karamba

This section describes a logical way of model a structure with Grasshopper and a structural analysis with tools from Karamba. It is the same procedure when modelling any kind of structure in the program. In the example below, a simply supported beam is used to describe the procedure.

The first thing to do when modelling a beam in Karamba is to describe a line between two points and then convert it to a beam with the tool called "LineToBeam". The length of the beam is determined by a number slider as seen in Figure 5.5, the "Move" tool creates a copy of the initial point that is movable.

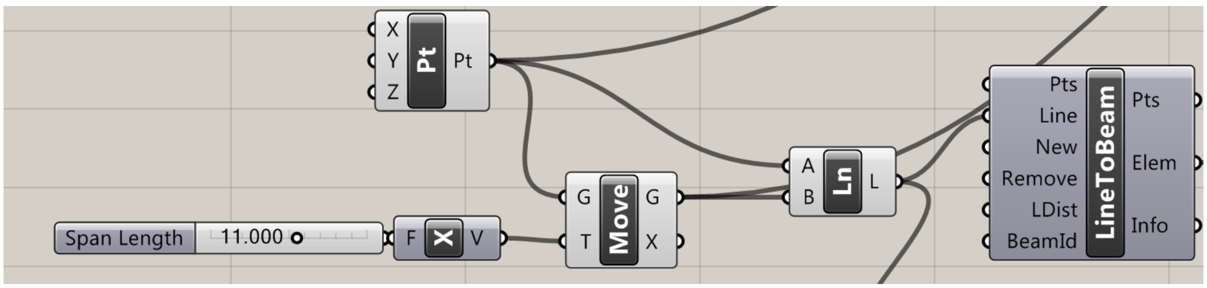

Figure 5.5: Visualisation of creating a beam in Karamba.

Next step is to create boundary conditions, supports, and decide which loads the beam is subjected to. All the information (geometry, supports and loads) is inserted in the "Assemble" tool. It is possible to give the model information about cross-section and material if a material dependent result is needed.

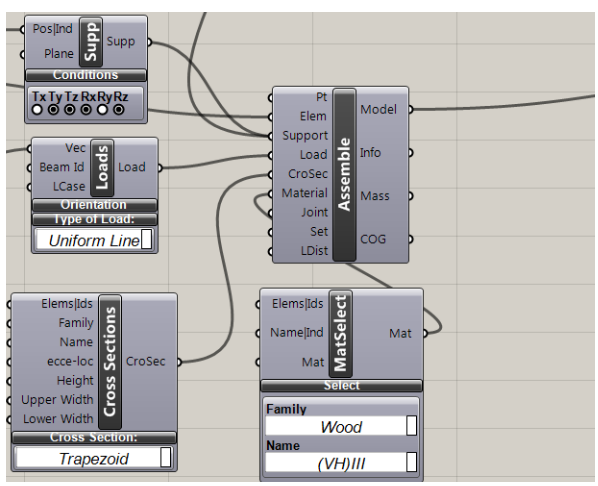

Figure 5.6: Applying loads and assigning boundary conditions in Karamba.

The last thing to do is to analyse the beam and display the results in a proper way. This can be achieved with the following configuration.

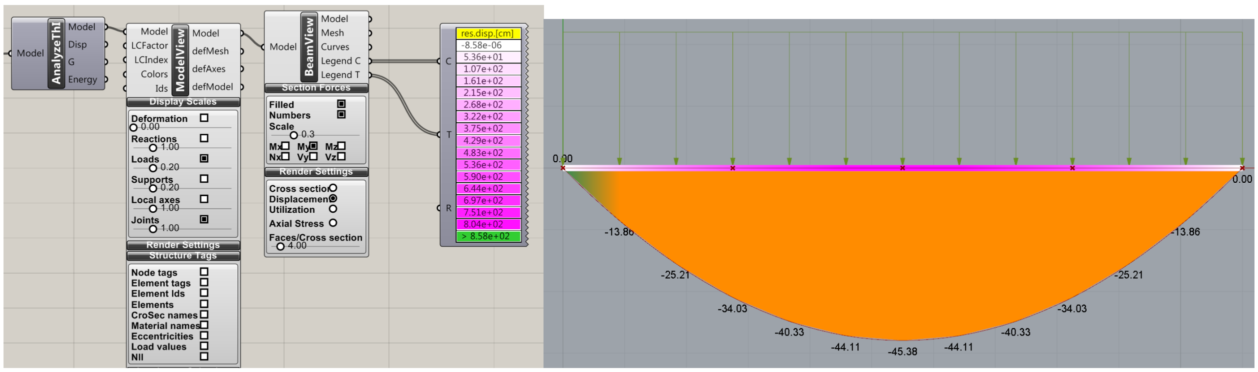

(a) The Karamba model (b) Visualisation of the bending moment diagram.

Figure 5.7: Results given by Karamba, bending moment and displacements.

5.3.2 Abaqus

The FE-software Abaqus is a tool to analyse 1, 2 and 3D problems. The basic of the analysis is based on the finite element method, described in Section 5.1. In Abaqus analysing of e.g. beam, shell and truss elements can be performed. The modelling procedure starts with creating of parts. The parts are then assigned with material properties and then assembled together. Thereafter, boundary conditions and loads are applied. Before running the analysis, the structure is meshed into finite elements.

Modelling procedure of the Stress Ribbon structure in Abaqus

In order to model the stress ribbon structure in Abaqus, beam elements are used, in order to achieve inherent bending stiffness. 1D elements are used in the model and the cable is divided into 49 elements. The boundary conditions at the supports are hinged. The load is applied in the vertical direction and therefore the anisotropic behaviour of the timber has not been taken into account in this case.

The beam orientation carefully needs to be studied individually since the normal direction of each element is approximate and cause Abaqus to use incorrect geometry for the analysis. Therefore an analytical calculation of normal direction has to be specified in the keywords editor (SIMULIA, 2017). To simplify the procedure, segments are created consisting of a number of elements. To account for geometrical non-linearity the function NLgeom has to be activated, which in this case account for large deformation between the nodal points. Especially in asymmetric load-cases the NLgeom has to be activated where large nodal deformations are obtained.

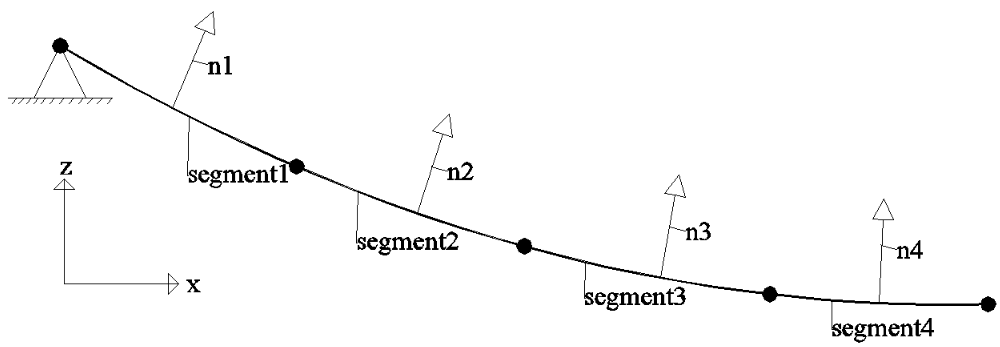

Figure 5.8: Illustration of how the normal direction is directed along the cable.

5.3.3 Discussion for choice of analysis program

Karamba is an easy to use FE-program with a visual way of modelling structural elements. To change parameters is fast and the program directly shows the result. In an early design phase Karamba forms a powerful design tool. However, for more complex structures as the stress ribbon where non-linearity needs to be included, Karamba does not give reliable results. Abaqus is, on other hand, a well known and experienced FE-program for structural engineers. Though Abaqus is not that user-friendly as Karamba, analysis for the final results are done with that software. The main reason for this is the more accurate results compared to the results provided from Karamba.

6 Loads on Stress Ribbon structures

Stress ribbon structures and tension structures in general have a much higher ratio between live and dead load compared to traditional beam system. The low self-weight gives the stress ribbon system the ability to span over long distances. Consequently, the structure gets more vulnerable to environmental actions as wind and snow loads (Rizzo, D'Asdia, Ricciardelli, & Bartoli, 2012).

In this chapter relevant loads acting on a stress ribbon roof structure are presented. How different loads act on the roof structure and what form they take is also discussed. Usually it is wind and snow loads that affect the design of a cable roof structure (Buchholdt, 1999). Other loads that affect the design of a stress ribbon structure are e.g. prestress force, live load and erection or temporary load during construction.

6.1 Self-weight

Load bearing members, in this case the stress ribbon, but also non-structural members such as roof cladding, service installations e.g. ventilation ducts or water pipes are included in the self-weight of the structure. The different parts that are included in the self-weight should be considered as one load in the load combination, SS-EN 1991-1-1 (CEN, 2011). Self-weight act in the same direction as the gravity.

6.2 Snow load

As there are no special regulations for a catenary shaped roof in SS-EN 1991-1-3 (CEN, 2005), a special investigation is required. According to SS-EN 1991-1-3 (CEN, 2005) factors that influence the distribution of snow on a roof are:

- The shape of the roof
- The thermal capacity of the roof
- The roughness of the surface
- The amount of heat produced under the roof
- Distance to nearby buildings
- The surrounding terrain
- The local climate i.e. the wind situations in the area and amount of precipitation

The most similar case to the catenary roof structure found in SS-EN 1991-1-3 (CEN, 2005) is the multi-span roof, as seen in Figure 6.1. The volume between the two roof-ridges forms a gap where snow can be gathered and might be a good approximation of the snow behaviour on the catenary roof. A similar approach has been used in a previous Master's thesis by Karnik (2007) and also discussed and confirmed by Pär Gustavsson[1].

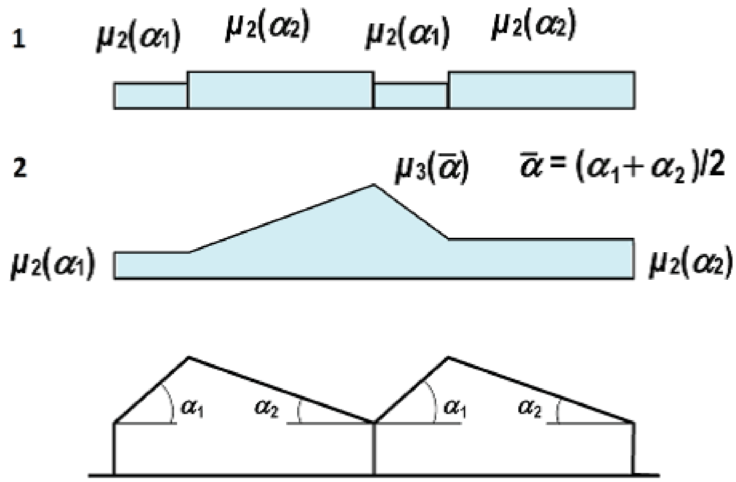

Figure 6.1: Multi-span roof subjected to snow load according to SS-EN1991-1-3 CEN (2005).

Snow drift on the roof structure is affected by the shape of the roof and the direction and velocity of the wind. Wind tunnel test may be an appropriate solution in order to see the behaviour of the snow drift and find problematic areas on the roof.

As the roof-ridges are placed with an equal height above the ground, the snow load according to SS-EN 1991-1-3 (CEN, 2005), is applied with a symmetrical shape. SS-EN 1991-1-3 (CEN, 2005) propose two different snow load distributions, one uniform and another with a triangular shape. Both alternatives need to be investigated with its respective shape coefficients, μ, to find the snow load. The μ-factor is determined from the slope of the roof, see Figure 6.1. As the slope is different in every section for the catenary roof structure it is an issue to choose angle. To use the highest angle, i.e the slope of the tangent at support section, gives a conservative amount of snow load, see area A3 in Figure 6.2. An alternative to get a more reasonable amount of snow load is to find the angle which gives the same area as the area for the triangle in alternative two in Figure 6.1, e.g. when area A1 and A2 are equal to each other, see Figure 6.2. In that case the load effect is equivalent to the total snow load given by SS-EN 1991-1-3 CEN (2005). However, in an early design phase it is reasonable to use the conservative value.

[1]Phone call 9:th March 2017, Manager of Technology and Business Development WSP Sverige AB

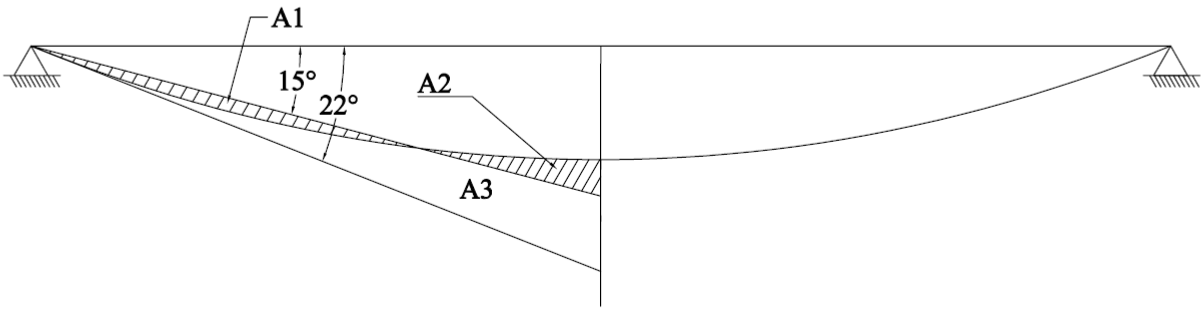

Figure 6.2: Approximation of slope of roof to find α.

This approach would for the reference building presented in Section 7.1.1 give an angle of 22°, which correspond to a μ_2 value equal to 0.8 and μ_3 value equal to 1.4.

In the case with a symmetrical shape of the stress ribbon structure, the maximum snow load is governed by alternative two, see Figure 6.1, which consequently gives the highest axial normal force and should be designed for.

6.3 Wind load

For common building shapes there are design information in standards and codes regarding wind loads. However for unusual shapes such as catenary shaped roof structures, no or little information is available. For such buildings Buchholdt (1999) suggests that wind tunnel tests together with computer analysis should be performed as early as possible.

The wind pressure (or suction) described in SS-EN 1991-1-4 (CEN, 2012) is acting perpendicular to or from the surface, see Figure 6.3.

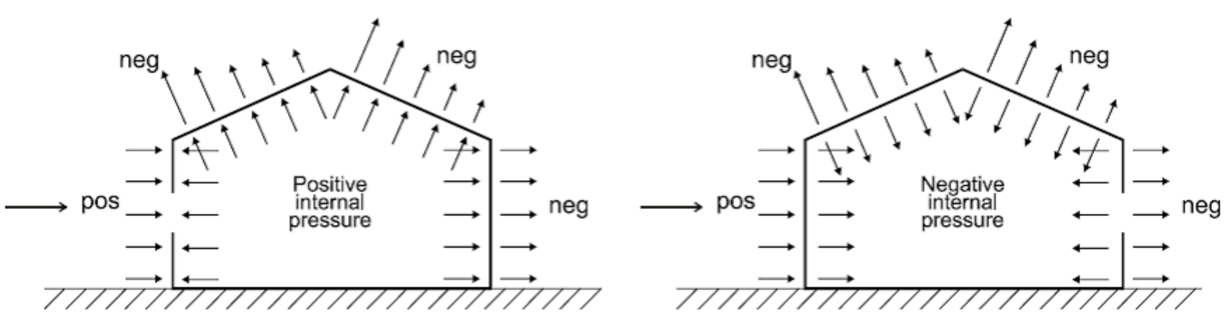

Figure 6.3: Direction of wind pressure according to BS-EN 1991-1-4 (CEN, 2012).

The main factors that affect the behaviour of a cable roof when subjected to wind are according to Elashkar and Novak (1983) wind turbulence, air enclosed underneath the roof, the shape, mass and dimensions and the pressure due to roof movements. Two wind tunnel tests were carried out by Elashkar and Novak (1983), one with a flat roof and another with a hyperbolic paraboloid shaped roof. When testing the hyperbolic paraboloid shaped roof, the pressure coefficient always acted in a negative direction, i.e. upward, except when high wind velocities were projected. The tests showed that the maximum response is not necessarily positioned in the centre point of the roof. For the test of the flat roof it was concluded that the maximum response was not located at the centre point of the roof. Conclusions to these tests are that the effect of the wind is hard to predict and the response is dependent on the roof slope.

Experimental values on wind loads have been investigated for cable roofs with hyperbolic paraboloid shape. Rizzo, D'Asdia, and Lazzari (2009) describes a wind tunnel test performed on a rectangular hyperbolic paraboloid shaped building, with wind direction towards both the long and short facade. Similarities in geometry can be found with the shape of the catenary, if studying the case with wind direction against the long facade, see Figure 6.4.

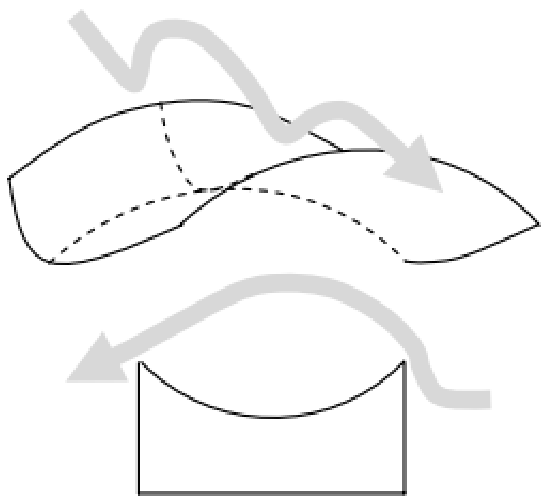

Figure 6.4: Wind direction of 90° in test by Rizzo, D'Asdia, and Lazzari (2009).

According to Magnusson (1985) the static wind pressure could be determined by wind tunnel tests. SBN (Swedish Building Norm) states that if $\tan(B) < 0.4$, where B is the slope of the roof, only wind suction needs to be taken into account during design (Magnusson, 1985). For a building with a span of 24 m and an initial sag of 2.5 m $\tan(B) \approx 0.4$, which according to SBN correspond to wind suction over the whole roof. The locally high suction forces that arise close to the boundary, within 1/10 of the width of the building, need just to be taken into consideration when designing the connections of the outer roof cover according to SBN.

A wind tunnel test was carried out on a scale model of Nagano Olympic Memorial Arena, described in Section 2.1.4, by Suzuki, Sanada, Hayami, and Ban (1997). The model of the arena was subjected to wind load towards the long façade and the result showed that the wind pressure was almost the same on every roof unit. Figure 6.5 displays the wind force coefficients from the wind tunnel test of the arena. It can be observed that a negative wind pressure covers the whole area of the roof structure.

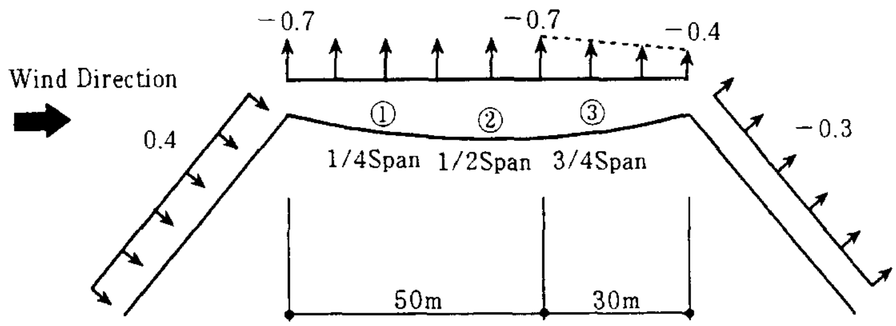

Figure 6.5: Mean wind force coefficient for static analysis of Nagano Olympic Memorial Arena (Suzuki, Sanada, Hayami, & Ban, 1997).

In SS-EN 1991-1-4 (CEN, 2012), section 7.2.5 the wind pressure coefficients for duo pitched roofs are presented. There are some similarities with the negative duo pitched roof, see Figure 6.6 and a catenary roof structure. Wind tunnel tests by Elashkar and Novak (1983), Rizzo et al. (2009), Suzuki et al. (1997) and SBN's recommendation all prove suction forces developed from the wind acting on a cable roof structure, which are possible to compare with the negative values from Table 6.1 and 6.2 from SS-EN 1991-1-4 (CEN, 2012). Therefore, an assumption to treat the wind loads on a catenary structure as a negative sloped duo pitched roof as described in SS-EN 1991-1-4 (CEN, 2012) might be reasonable. For a cable shaped roof with a span of 24 m and sag of 2.5 m the average angle is (-12°). According to SS-EN 1991-1-4 (CEN, 2012) roofs are considered flat if the slope is below +/- 5°.

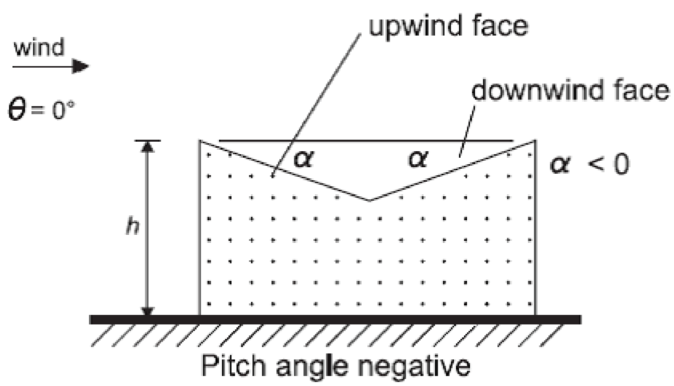

Figure 6.6: Negative sloped duo pitched roof.

6.3.1 Comparison and Conclusion

In this section a comparison between the tests will be displayed and with this data a conclusion is drawn on how to handle wind loads in a static preliminary design state. The tests and standards described in the previous section proves that suction will be the dominating force acting over the catenary roof structure. If the sag of the catenary roof structure is small, an alternative is to compare the wind pressure coefficients for a flat roof. The comparison is done with the wind pressure coefficients from:

(a) Rizzo et al. (2012) hyperbolic paraboloid roof with wind at 90°, see Figure 6.4

(b) Suzuki et al. (1997) Nagano Olympic Memorial Arena with wind against the long façade, see Figure 6.5

(c) An approximation of the wind on a duo pitched roof with negative slopes (-12°) according to SS-EN 1991-1-4 (CEN, 2012), see Figure 6.6

(d) Wind acting on a flat roof according to SS-EN 1991-1-4 (CEN, 2012)

In all these tests, the wind is acting perpendicular to the facade belonging to the lowest parts of the roof and consequently possible to compare. The wind pressure effects closest to the corners are not considered in this comparison. Though Rizzo et al. (2012) state that ”It is clear that the peculiar shapes of tensile structures make it impossible to use the pressure coefficient values available for flat, pitch or vaulted roofs” (p.61) it is still possible to see a general behaviour of the wind action.

To do the comparison a reference building is established with a span length of 24 m and sag of 2.5 m, the maximum slope (at support section) is approximately 22° and obviously 0° at mid span. The width of the building perpendicular to the span is set to 24 m, this is done because the model of the hyperbolic paraboloid was square shaped. The results are presented in Figure 6.7.

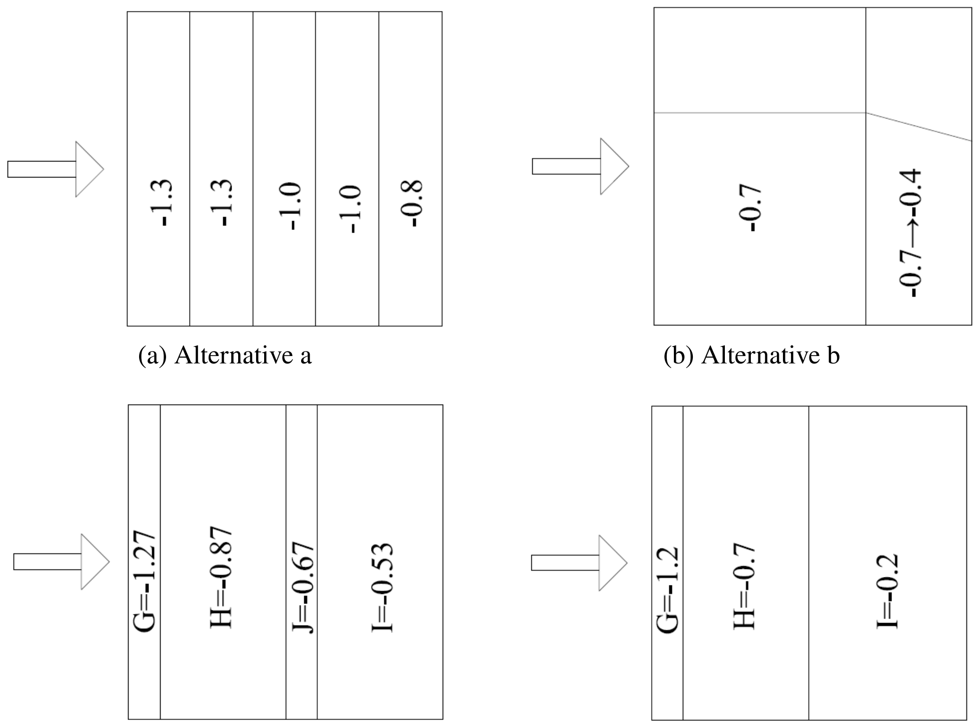

(a) Alternative a (b) Alternative b

(c) Alternative c (d) Alternative d

Figure 6.7: Shows the wind pressure coefficients from a) Test on a hyperbolic paraboloid shaped structure, b) Wind tunnel test on a model of Nagano Olympic Memorial Arena, c) SS-EN 1991-1-4 (CEN, 2012) on a negative slope duopitched roof (-12°) and d) SS-EN 1991-1-4 (CEN, 2012) on a flat roof with sharp eaves.

The lack of relevant experimental reports on hanging roof structures makes this comparison not that accurate. A comparison with more tests would make a more reliable assumption of the wind action on the roof. However, it is possible to use these test results of the wind action in a preliminary design. For the final design wind tunnel tests are beneficial in order to find the real behaviour of the wind action on the catenary structure. The test results of Nagano Memorial Olympic Arena are the only tested model with the actual catenary shape. The test shows the most favourable numbers when it comes to wind suction on the roof, a reason for this can be the inclined walls that reduce the turbulence effect. Furthermore, the wind pressure coefficients are acting in a vertical direction, see Figure 6.5, in contrast to what is stated in CEN (2012) where the wind is acting perpendicular to the roof.

In Table 6.1 and 6.2 it can be seen that a negative wind pressure is acting on the duo pitched roof independent on wind direction (except for part I and J for a small slope with wind at 0°), this also confirms the tests made by Elashkar and Novak (1983).

Table 6.1: Recommended values of external pressure coefficients for duopitch roofs with wind direction of 0°, according to SS-EN 1991-1-4 (CEN, 2012)

Pitch Angle α	Zone for wind direction $\theta = 0°$									
	F		G		H		I		J	
	$c_{pe,10}$	$c_{pe,1}$	$c_{pe,10}$	$c_{pe,1}$	$c_{pe,10}$	$c_{pe,1}$	$c_{pe,10}$	$c_{pe,1}$	$c_{pe,10}$	$c_{pe,1}$
-45°	-0,6		-0,6		-0,8		-0,7		-1,0	-1,5
-30°	-1,1	-2,0	-0,8	-1,5	-0,8		-0,6		-0,8	-1,4
-15°	-2,5	-2,8	-1,3	-2,0	-0,9	-1,2	-0,5		-0,7	-1,2
-5°	-2,3	-2,5	-1,2	-2,0	-0,8	-1,2	+0,2 -0,6		+0,2 -0,6	

Table 6.2: Recommended values of external pressure coefficients for duopitch roofs wind direction of 90°, according to SS-EN 1991-1-4 (CEN, 2012)

Pitch angle α	Zone for wind direction $\theta = 90°$							
	F		G		H		I	
	$c_{pe,10}$	$c_{pe,1}$	$c_{pe,10}$	$c_{pe,1}$	$c_{pe,10}$	$c_{pe,1}$	$c_{pe,10}$	$c_{pe,1}$
-45°	-1,4	-2,0	-1,2	-2,0	-1,0	-1,3	-0,9	-1,2
-30°	-1,5	-2,1	-1,2	-2,0	-1,0	-1,3	-0,9	-1,2
-15°	-1,9	-2,5	-1,2	-2,0	-0,8	-1,2	-0,8	-1,2
-5°	-1,8	-2,5	-1,2	-2,0	-0,7	-1,2	-0,6	-1,2

With a similar procedure as when the snow load was selected, the roof is designed for the worst scenario. In this case it is governed from the highest up-lift force. Therefore, the structure should in an early stage be designed according to alternative (a) in Figure 6.7. Furthermore, alternative (a) has a distribution of wind pressure coefficients similar to the coefficients from Nagano Olympic Memorial Arena which makes it reliable.

6.4 Load Combination

As any other structure, a cable shaped roof needs to be designed with regard to both ultimate strength and serviceability (Krishna, 2015), this corresponds well to what SS-EN 1990 (CEN, 2010) states i.e. two different states of design, ultimate limit state and serviceability limit state. In this section the most unfavourable load combinations in design are discussed.

6.4.1 Critical Load Combinations

To ensure that a cable without bending stiffness never become slack i.e. compressive axial forces are introduced in the system the uplifting force from wind action should never exceed the self-weight. The stress ribbon system is designed to withstand tensile forces and the risk of buckling in the slender elements is major. The governing equation for this condition to occur in this study corresponds to eq. (6.10) in SS-EN 1990 (CEN, 2010) where the self-weight is reduced with 10%, the snow load is considered as favourable and consequently equal to zero and the uplifting wind load is increased by 50%. This combination gives the maximum uplift force and should therefore be taken into consideration for design. For a system with bending stiffness compressive forces are allowed as long as they do not exceed the buckling strength of the element.

The load case which gives the highest axial tensile stresses in the stressed ribbon structure needs to be checked. According to Krishna (2015) is the cable designed to sustain the tensile strength in the worst loaded case, with included partial factors. The worst case of eq. (6.10a) and (6.10b) in SS-EN 1990 (CEN, 2010) should be considered in the ultimate limit state.

$$q_{d.6.10a} = \gamma_d \left(1.35 G_{kj,sup} + 1.5 \sum \psi_{0,i} Q_{k,i} \right) \tag{6.10a}$$

$$q_{d.6.10b} = \gamma_d \left(0.89 \times 1.35 G_{kj,sup} + 1.5 Q_{k,1} + 1.5 \sum \psi_{0,i} Q_{k,i} \right) \tag{6.10b}$$

The γ_m factor is a safety factor which depends on the reliability class. The factor $G_{kj,sup}$ represents the permanent load while $Q_{k,i}$ represent the variable load with its corresponding combination factor $\psi_{0,i}$, acting on the structure.

The stress ribbon has a small cross-section compared to the length of the span causing the structure to be very flexible and sensitive to asymmetric loads. A check in serviceability limit state needs to be performed. In this study the characteristic load case is chosen because it does not reduce variable load and consequently gives the largest deformations.

7 Analysis of the Stress Ribbon structure

In order to design the stress ribbon structure for realistic load cases, a verification between three analytical and numerical solutions are presented. Then a preliminary design of the structure is performed with results gathered from FE-analyses, and finally a check of the utilisation ratios for the stress ribbon structure are presented.

7.1 Verification of analysis method

In order to design the stress ribbon structure for realistic load cases, a suitable analysis method is desirable. In this section, three different load cases are used to compare analytical- and numerical solutions to find a suitable analysis tool.

7.1.1 Case study

Three analysis methods are carried out in this thesis, one analytical, one in Karamba/Grasshopper and one in ABAQUS. The structure is divided into 49 elements. A convergence study of the numbers of elements for the structure is performed. The result for this case indicated that more than 49 elements would not affect the structure significantly. A case study with 36 m span length is also performed in order to verify the model for different span lengths. This resulted in similar proportions for deflection and sectional forces as the case for 24 m span length.

A reference building located in Stockholm is establish with the following input data, span-length 24 m, maximum sag 2.5 m, glulam elements with a spacing of 0.8 m, class GL30h and cross-section 78 x 180 mm^2. The loads are self-weight and imposed load applied on the structural elements. The imposed load is distributed in three special cases, see Figure 7.2. The load is also applied in two different configurations, line load and equivalent node load, for the cases with uniform and asymmetrical load distributions, see Figure 7.1. This is done to compare and recognise if there are any major differences of the behaviour when the load is applied in different manners.

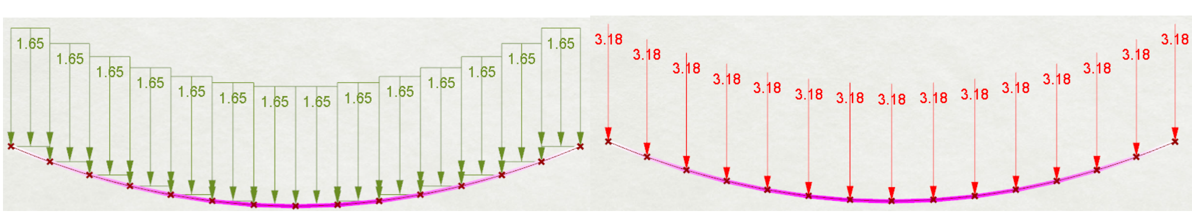

(a) (b)

Figure 7.1: The cable is subjected to, a) line load, b) equivalent node load.

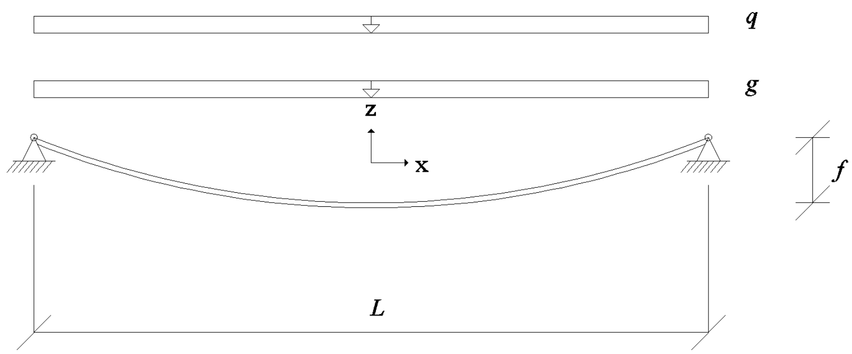

(a)

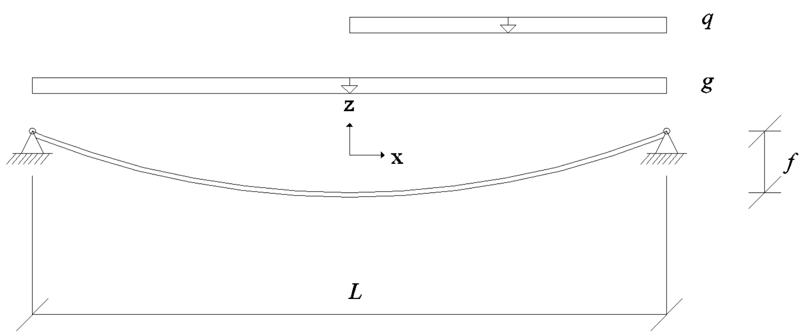

(b)

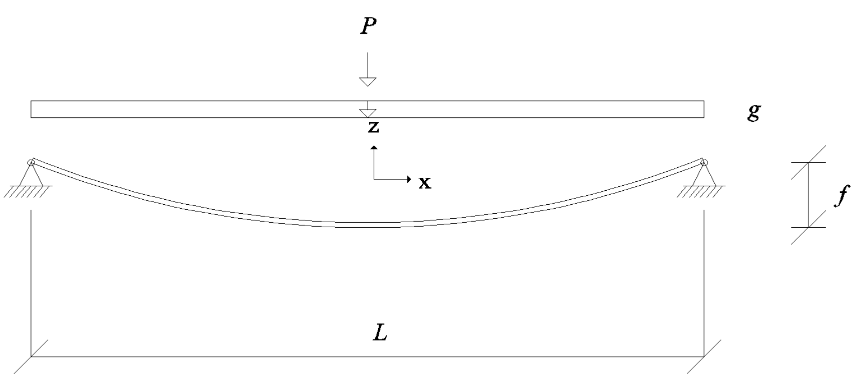

(c)

Figure 7.2: Distribution of imposed load (a) Uniformly distributed along the whole span, (b) Asymmetric load applied in half of the span, (c) Point load applied at mid-span.

7.1.2 Conclusion on analysis method

The difference between the results from numerical and analytical methods are given in Table 7.1. It can be seen that the normal force for both of the FE-analyses corresponds well to the analytical solution. The reaction forces for all different cases also agree with the analytical method. This proves that the loads are placed at their right position with an equal magnitude and make the models reliable.

The moment distribution for uniform load in the Karamba model is unreasonable regardless of the load application, an example of this is shown in Figure 7.3. For asymmetric load cases the moment distribution is reasonable independent if the loads are applied as line or node loads but they are a lot higher than for the analytical solution. Karamba also gives displacements about four times higher than the analytical solution when comparing the asymmetrical load case. The model in Karamba does not handle geometrical non-linearity and that can be an explanation to the high deflections. These derivations make the Karamba model untrustworthy even if the axial stresses correspond well.

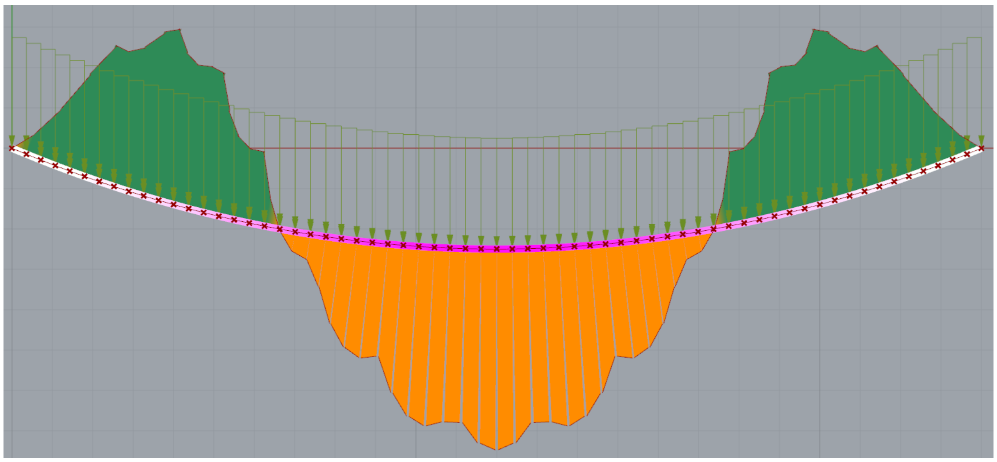

Figure 7.3: Unreasonable moment distribution, displayed from Karamba.

A comparison between the Abaqus analysis and the analytical solution shows a significant difference in deflection, about 50% in the load cases with uniform load and central point load. For the asymmetrical load cases the downward deflection is reduced and deviate with 14% while the upward deflection deviate with approximately 7% from the analytical solution. The reasons behind the large differences when comparing deflections are remarkable, since other results correspond well. The moment distribution when a uniform node-load is applied gives a unreasonable result. The reason for this is the uneven division of nodes along the stress-ribbon length. The nodes are divided with an equal distance along the x-direction which implies a more dense distribution of nodes when approaching mid-span of the cable and consequently gives a higher load.

The analysis shows that asymmetric loads have a great influence on the behaviour of a slender and flexible element as a stress ribbon. Displacements and bending moments increase for just a small eccentricity of the load. All values for each analysis method for the verification process are presented in Appendix F.

Preliminary design and the results presented in Section 7.2 are obtained from an Abaqus analysis. Though Abaqus show a big deviation in deformation from the analytical solution it is used. The major reason of this choice is the demand to handle geometrical non-linearity.

Table 7.1: Percental difference of deflections and forces between numerical and analytical solutions. Green boxes imply less than 5% difference, yellow between 5% and 20% and orange over 20% difference.

(a)

Abaqus/analytical	1, Uniform line-load	2,Uniform node-load	3, Assymetric line-load	4, Assymetric node-load	5, Central point-load
Max Normal Force [kN]	102%	98%	89%	84%	100%
Min Normal Force [kN]	102%	98%	101%	95%	102%
Max Pos Moment [kNm]	158%		89%	90%	86%
Max Neg Moment [kNm]			99%	97%	90%
Max ↓ Deflection [mm]	158%	173%	86%	86%	137%
Max ↑ Deflection [mm]			107%	106%	60%
Max Axial Stress [MPa]	102%	98%	89%	84%	100%
Reaction Force [kN]	103%	100%			103%

(b)

Karamba/analytical	1, Uniform line-load	2,Uniform node-load	3, Assymetric line-load	4, Assymetric node-load	5, Central point-load
Max Normal Force [kN]	101%	101%	85%	81%	96%
Min Normal Force [kN]	101%	101%	96%	91%	97%
Max Pos Moment [kNm]	546%	66%	323%	335%	121%
Max Neg Moment [kNm]			341%	337%	156%
Max ↓ Deflection [mm]	209%	66%	337%	344%	187%
Max ↑ Deflection [mm]			352%	354%	139%
Max Axial Stress [MPa]	101%	101%	85%	81%	96%
Reaction Force [kN]	100%	100%			100%

7.2 Design of the structure

A preliminary design of the cable is presented in the following section. Firstly, some material properties are stated according to SS-EN 1995-1-1 (CEN, 2009). Secondly, results from the two different load cases are presented, and finally an utilisation check of the material is performed.

7.2.1 Material properties - Glulam

In the following section are material properties for the glulam member in the design phase presented. In Table 7.2, characteristic material properties for glulam, GL30h, is presented.

Table 7.2: Characteristic material properties for glulam, GL30h.

Bending Strength, $f_{m,g,k}$	30.0 MPa
Tensile strength, $f_{t,0,g,k}$	24.0 MPa
Modulus of elasticity, $E_{0,g,mean}$	13.6 GPa
Density, $\rho_{g,mean}$	4.8 kN/m^3

The design strength values for the Glulam ribbons are according to SS-EN 1995-1-1 (CEN, 2009), calculated as

$$R_d = k_{mod} \frac{R_k}{\gamma_m}$$

- R_d - Design strength value
- R_k - Characteristic strength value
- k_{mod} - Modification factor for duration of load and moisture content
- R_d - Partial factor for material property

Determination of the modification factor k_{mod} in SS-EN 1995-1-1 (CEN, 2009) is based on the load duration class and service class. The Load duration class for snow is assumed to be medium term action, and service class 1 is assumed. This give the following value of k_{mod}

$$k_{mod} = 0.8$$

The partial factor is equal to

$$\gamma_m = 1.25$$

Members in tension or bending will be modified by a factor k_h according to SS-EN 1995-1-1 (CEN, 2009). This factor consider the size of the section, where members in tension with a width smaller than 600 mm and for members in bending with a height smaller than 600 mm are modified by the additional factor.

$$k_h = min\left(\left(\frac{600}{h}\right)^{0.1}, 1.1\right)$$

- h - Height for members in bending. width for members in tension [mm].

The design of the modulus of elasticity is according to SS-En 1995-1-1 (CEN, 2009), stated as

$$E_d = \frac{E_{mean}}{\gamma_m} \tag{7.1}$$

In the design in ULS, consideration of creep should be accounted for, if the distribution of member forces is affected by the stiffness distribution according to SS-EN 1995-1-1 (CEN, 2009). The modulus of elasticity is calculated as

$$E_{mean,fin} = \frac{E_{mean}}{1 + \psi_2 k_{def}}$$

- ψ_2 - Factor for quasi-permanent load
- k_{def} - Creep factor

7.2.2 Results

Results from Abaqus analysis are described in this chapter when realistic load cases are applied on the stress ribbon structure. The loads presented in Chapter 6 are applied on the structure with their actual shape, direction and size. The most critical load cases, discussed in Section 6.4 are investigated, were eq. (6.10a) and (6.10b) are used.

The most vulnerable cases to be checked are given by the load combination which gives the highest stresses in the stress ribbon structure and the combination which gives the highest up-lift force. Calculations for loads are shown in Appendix C. As in the case study the following input data is: span-length 24 m, maximum sag 2.5 m, glulam elements with a spacing of 0.8 m, class GL30h and cross-section 78 x 180 mm^2.

Snow load

As concluded in Section 6.2 the snow load to be considered during design is alternative two (triangular shaped) according to Figure 7.4. The relative deformation, i.e. the deformation from its original position, when snow load is acting on the structure is displayed in Figure 7.5. Deformation when only self-weight is applied is also shown in Figure 7.5 to give an understanding of the behaviour of the structure unloaded. The real deformation behaviour is displayed in Figure 7.6. The two curves represent the shape of the cable unloaded and when snow load is acting. Normal force along the stress ribbon element when snow load is applied is shown in Figure 7.7. The highest normal forces occur closest to the supports as expected.

The building is assumed to be placed in Stockholm, Sweden. The characteristic snow load is given as

$$s_k = 2.0kN/m^3$$

According to SS-EN 1991-1-3 (CEN, 2005), the snow load should be multiplied by a factor which consider the geometry of the roof. The shape factors are assumed as

$$\mu_2 = 0.8$$

$$\mu_3 = 1.4$$

And for the load combination the partial factor ψ_0 is equal to

$$\psi_{0,s} = 0.7$$

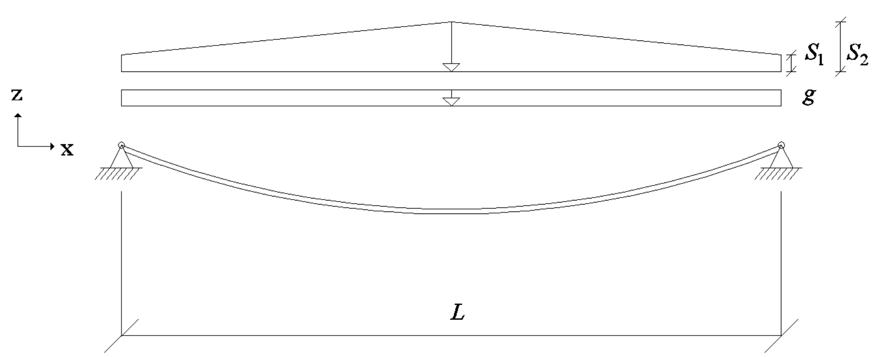

Figure 7.4: Design snow load distribution where S_1 and S_2 are the snow load obtained from μ_2 and μ_3 respectively, according to Figure 6.1.

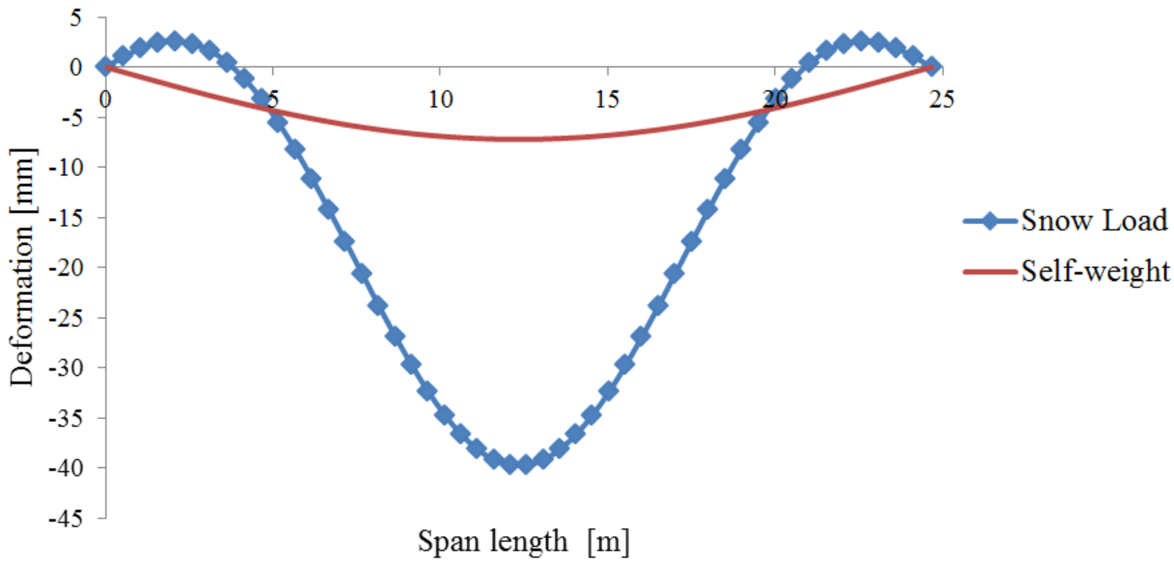

Figure 7.5: The relative deformation when the stress ribbon structure is subjected to snow load.

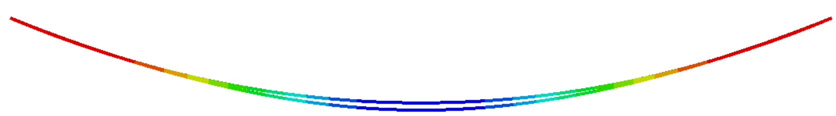

Figure 7.6: Deformation figure from Abaqus when snow load is applied, deformation scale factor set to 4.0. The upper curve represent the original position of the cable and the lower when designed snow load is applied.

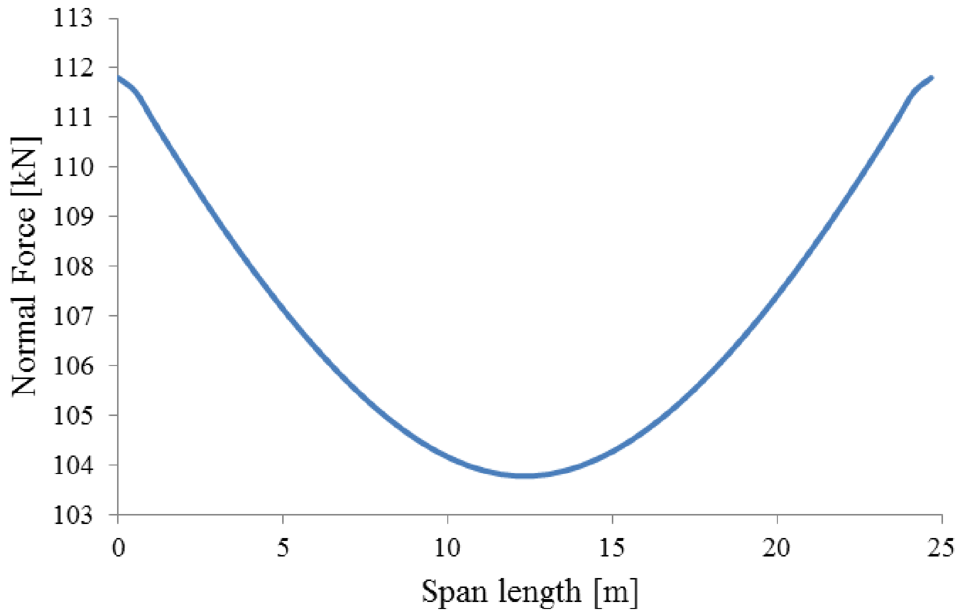

Figure 7.7: Normal force distribution along the span length.

Wind load

The highest up-lift forces arise when wind pressure coefficients according to option (a) in Section 6.3.1 are used. The wind pressure distrubition that acts on the stress ribbon element is shown in Figure 7.8. Relative deformation and normal force distribution are shown in Figure 7.9 and Figure 7.11 respectively. The real deformation behaviour is shown in Figure 7.10. The asymmetrical wind load force the cable to rise in the left parts of the span and consequently drop in the right parts. As already concluded in Section 7.1.2 asymmetrical loads result in large vertical deformations. A confirmation of this is shown in Figure 7.9 where an asymmetrical wind load is applied. Compare this with the case with symmetrical snow load and it is obvious that the asymmetrical wind loads provide larger deformations, even though the applied wind load is smaller. Figure 7.11 displays that compressive forces are introduced in the structure when wind load is acting. Risks that arise with these forces are buckling. A buckling strength calculation is carried out and the result shows there are no risk of buckling, see Appendix D.

The wind speed according to SS-EN 1991-1-4 in Stockholm is:

$$v_b = 24m/s$$

The terrain category is assumed to be level III and the height of the building to 15 m.

The external wind pressure coefficients are

$$c_{pe1} = -1.3 \qquad c_{pe2} = -1 \qquad c_{pe3} = -0.8$$

for respectively load q_1, q_2 and q_3 according to Figure 7.8.

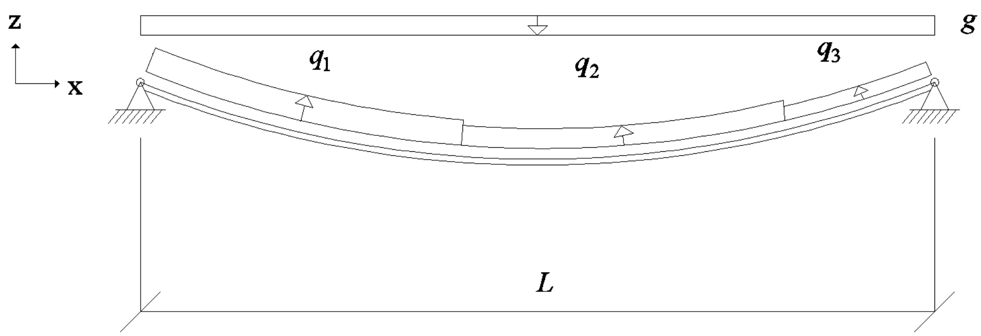

Figure 7.8: Designed wind load distribution.

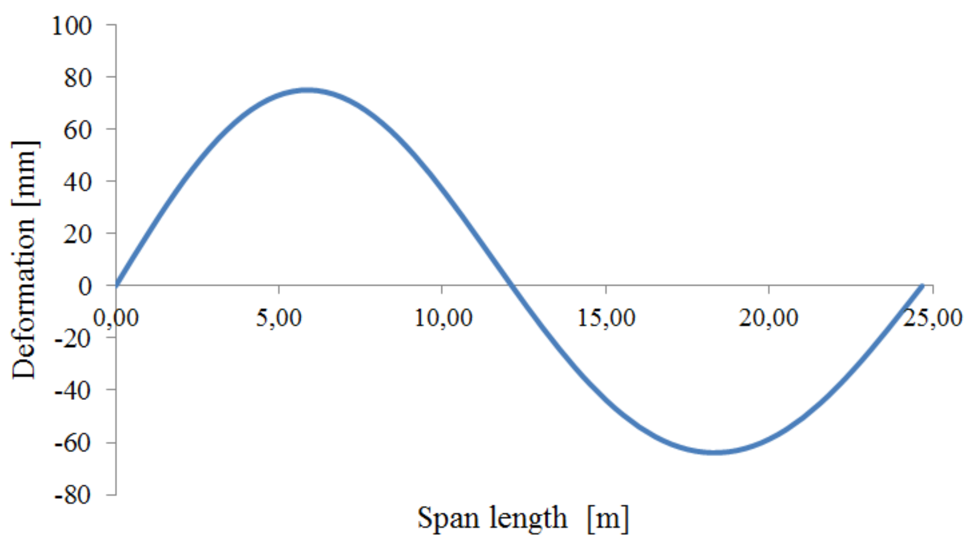

Figure 7.9: Relative deformation when the stress ribbon structure is subjected to wind load.

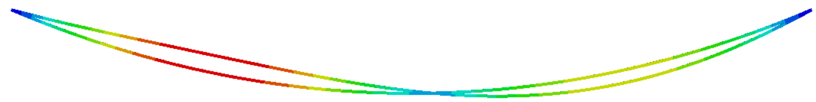

Figure 7.10: Deformation figure from Abaqus when wind load is applied, deformation scale factor set to 4.0. The figure shows the original shape of the stress ribbon when wind load is applied.

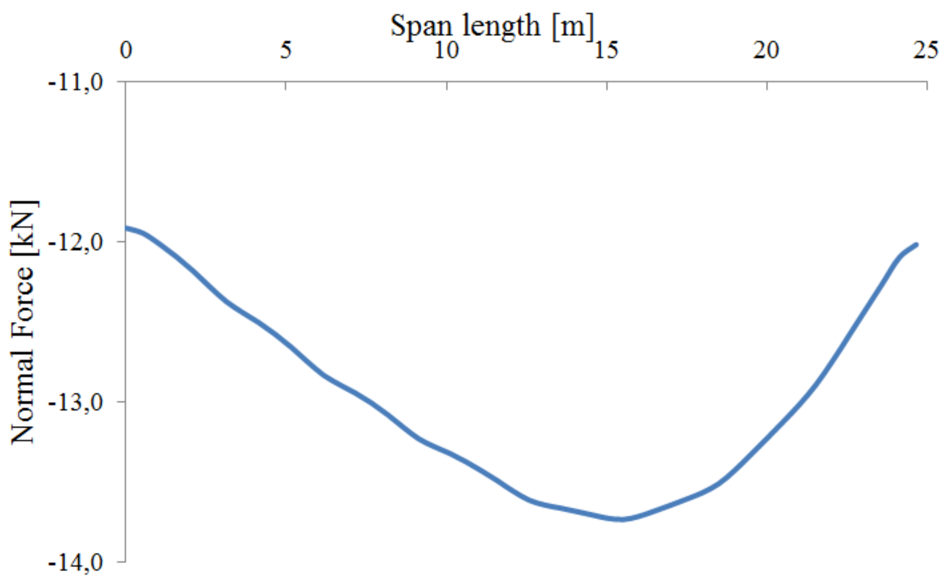

Figure 7.11: Normal force distribution along the the span length.

The largest deformation appears when the structure is subjected to wind load. In Figure 7.9 the highest deformation is around 75 mm which correspond to the applicable limit $L/300 = 80$ mm for a span length of 24 m.

Utilisation ratios

A check of the utilisation of the timber in the analysis for the two design cases are presented in Table 7.3 according to SS-EN 1995-1-1 (CEN, 2009). The first parameter that is checked is deflection:

$$\delta \leq \frac{L}{300} \tag{7.2}$$

secondly, the utilisation in tension is checked:

$$\sigma_{t.0.d} \leq f_{t.0.d} \tag{7.3}$$

thirdly, the utilisation in bending:

$$\sigma_{m.0.d} \leq f_{m.0.d} \tag{7.4}$$

and for wind case the check of the buckling capacity is performed due the uplifting force of the cable.

$$N_d \leq N_{cr} \tag{7.5}$$

In the case when there are both axial tension and bending acting on the cable, the following requirement needs to be fulfilled.

$$\frac{\sigma_{t.0.d}}{f_{t.0.d}} + \frac{\sigma_{m.y.d}}{f_{m.y.d}} \leq 1$$

Table 7.3: Utilisation ratio for the Stress Ribbon structure.

	Snow load	Wind load
Deflection	0.5	0.94
Tension	0.47	0.06
Bending	0.12	0.72
Buckling	-	0.54
Combined	0.56	0.77

8 Discussion

The relation between cross-section and span length of a stress ribbon structure makes it sensitive to asymmetrical loads that consequently create large deformations. How to connect the stress ribbon roof to the facade with these large deformations is an issue. Other issues are the connection to e.g. ventilation ducts and sprinkler systems, that often are positioned just below the roof. There are different alternatives to reduce the deformations, e.g. increase the self-weight or increase the stiffness in the system. A way to increase the self-weight can be to change the roofing material to a material with higher density or create roof landscaping by putting ground material on the roof. To increase the stiffness, pretension cables can be used.

Roof structures with the shape of a cable are not covered in Eurocode. However, to preform a preliminary design of a stress ribbon structure, load distributions for snow and wind are presented in Chapter 6. The recommendations to use the most conservative load case in design, cause the structure to be designed conservatively but can imply a unnecessary use of material.

In this thesis an equal height of the two roof-ridges were assumed causing the snow load to be applied with a symmetrical shape on the roof. Different heights of the roof-ridges create different load configurations that could imply asymmetrical distribution of snow load. There is an existing risk of snow drift for the roof shape at hand. This can result in load distributions, not covered in CEN (2005), that are possible to occur. Unexpected load cases needs to be investigated with wind tunnel tests. As concluded in Section 7.2, asymmetrical loads develop great deformations and are therefore harmful to the system.

Wind load is an unpredictable load and therefore needs to be investigated for each special case. As discussed in Section 6.3, the most unfavourable wind pressure coefficients from the four presented alternatives were chosen for the analysis. If a wind tunnel test displays even higher wind pressure coefficients, the risk of buckling in the timber members are increased. Furthermore, higher wind loads imply greater deformations of the roof structure, greater uplift force and consequently a heavier substructure is required.

Two different FE-analysis programs, ABAQUS and Karamba, were evaluated for the analysis of the stress ribbon structure. The large deviation between Karamba and the analytical solution makes the choice of not using Karamba decisive. The comparison between ABAQUS and the analytical solution gave more similar results. On the other hand, the deformations and the moment comparison had some clear deviations.

Since no test model has been built, no practical test has been performed during the work with this thesis. The comparison between the different analysis methods indicate that ABAQUS can be used for a preliminary design of a stress ribbon structure. The results from the ABAQUS analysis, with realistic load cases applied, show good prospects for the stress ribbon structure. However, practical tests have to be performed in order to verify the concept. To increase the use of stress ribbon structures, norms and standards need to be created.

9 Conclusion

The aim of this study was to investigate how non-uniform loads affect the stress ribbon structure. Asymmetric load combinations will cause large deformations on the roof structure. This may cause problematic detail solutions which need to be further investigated. In order to design the stress ribbon structure for realistic load combinations, when snow or wind loads are acting on the roof, wind tunnel tests are preferable due to the uncertain distribution of the loads. In Chapter 6, recommendations to perform wind tunnel tests are suggested by different references.

The case study, where an analytical solution was compared with FE-analyses, indicates that normal force was similar in all cases. The study also shows a deviation when deformations are compared. Nevertheless, ABAQUS was chosen to do analyses with realistic load cases applied. Consideration of non-linearity in the structure is important since the ribbon is sensitive to deformations due to the small section compared to the span length, especially for asymmetric load cases. In order to verify the analytical and numerical solutions for the stress ribbon structure, a small test structure is recommended.

10 Further Studies

In this thesis the primary focus has been on how static load combinations affect the stress ribbon structure. As mentioned in Section 6.3, wind tunnel test is recommended due to the complexity to decide the pressure coefficients. Apart from static load combinations covered in this thesis, a number of recommended further studies are stated below.

- *Dynamic analysis* - This analysis is of importance since the small dimensions of the ribbons will lead to less rigidity as well as the self-weight will be low for each ribbon. The action from the wind will be most critical.
- *Wind tunnel test* - In order to have a reliable design of the stress ribbon structure a wind tunnel test is essential. As mentioned in Section 6.3 a more accurate analysis of the wind- and snow loads could be performed by wind tunnel tests.
- *Connections* - The splicing of the cable elements need to be further investigated. In Hofverberg (2016), finger joints is discussed while in Grandview Heights Aquatic Centre, paired glulam beams with an intermediate steel plate is used. However, calculation of splicing of the elements need further analysis.
- *Enviromental benefits* - In Hofverberg (2016), an investigation of the environmental impact was performed. However, further investigation of the stress ribbon system is necessary in order to compare the environmental impact depending on what kind of substructure that is used.

References

afaconsult. (2005). New braga municipal stadium, braga. *Structural Engineering International 2/2005*, *2*. (Cited on page 8).

Ban, S., Motohashi, S., Yoshida, A., & Tsubota, H. (1999). Dynamic characteristics of a semi-rigid hanging roof structure composed of glulams and steel plate. *Engineering Structures*. (Cited on pages 9, 10).

Brünninghoff, H. (1993). The essing timber bridge. *Structural Engineering International*. (Cited on pages 11, 12).

Buchholdt, H. A. (1999). *An introduction to cable roof structures*. Thomas Telford. (Cited on pages 16, 18, 32, 34).

CEN. (2005). *Ss-en1991-1-3. eurokod 1 – laster på bärverk – del 1-3: Allmänna laster – snölast*. Swedish Standards Institute. (Cited on pages 32, 33, 47, 53).

CEN. (2009). *Ss-en1995-1-1:2004. eurokod 5: Dimensionering av träkonstruktioner – del 1-1: Allmänt – gemensamma regler och regler för byggnader*. Swedish Standards Institute. (Cited on pages 18, 45, 46, 52).

CEN. (2010). *Ss-en 1990. eurocode – basis of structural design*. Swedish Standards Institute. (Cited on pages 39, 40).

CEN. (2011). *Ss-en1991-1-1. eurokod 1: Laster på bärverk – del 1-1: Allmänna laster – tunghet, egentyngd, nyttig last för byggnader*. Swedish Standards Institute. (Cited on page 32).

CEN. (2012). *Ss-en1991-1-4. eurocode 1: Actions on structures – part 1-4: General actions – wind actions*. Swedish Standards Institute. (Cited on pages 34, 36–39).

Dahlblom, O. & Olsson, K.-G. (2010). *Strukturmekanik, modellering och analys av ramar och fackverk*. Författarna och Studentlitteratur 2010. (Cited on pages 26, 27).

Elashkar, I. & Novak, M. (1983). Wind tunnel studies of cable roofs. *Journal of Wind Engineering and Industrial Aerodynamics*. (Cited on pages 34, 36, 38).

HCMA. (2016). Grandview heights aquatic centre. Retrieved from http://hcma.ca/project/grandviewheights/. (Cited on pages 3–5)

Hofverberg, S. (2016). *Long-span tensile timber roof structures* (Master's thesis, Chalmers University of Technology, Divison of Structural Engineering). (Cited on pages 1, 3, 12, 14, 15, 20, 55).

Jeska, S. (2014). Gessental bridge. *Emergent Timber Technologies*. (Cited on pages 5–7).

Jeska, S., Pascha, K., & Hascher, R. (2014). *Emergent timber technologies*. Birkhauser. (Cited on page 18).

Johansson, M. (2016). *Dimensionering av träkonstruktioner, del 1*. Svenskt Trä. (Cited on page 1).

Karnik, M. (2007). *Diskret ickelinjär analys av geometriskt föränderliga linsystem* (Master's thesis, KTH Royal Institute of Technology, Divison of Structural Engineering). (Cited on page 33).

Krishna, P. (2015). *Cable-suspended roofs, second edition*. McGraw-Hill Education LLC. (Cited on pages 16, 27, 28, 39, 40).

Linville, J. D. (2012). *Timber construction manual*. John Wiley and Sons. Inc. (Cited on page 18).

Magalhaes, F., Caetano, E., & Cunha, A. (2007). Operational modal analysis and finite element model correlation of the braga stadium suspended roof. *Engineering Structures*. (Cited on page 8).

Magnusson, K. (1985). Hängkonstruktioner. In S. Avén (Editor), *Handboken bygg konstruktionsteknik* (Chapter 25, Pages 488–492). Stockholm: LiberFörlag. (Cited on page 35).

Marti, P. (2013). *Theory of structures, fundamentals, framed structures, plates and shells.* Wilhelm Ernst and Sohn. (Cited on pages 20, 23).

Naturally-Wood. (2016). Grandview heights aquatic centre. Retrieved from http://www.naturallywood.com/project-gallery/grandview-heights-aquatic-centre. (Cited on pages 3, 4)

Ottosen, N. & Petersson, H. (1992). *Finite element method*. Prentice Hall. (Cited on page 25).

Preisinger, C. & Heimrath, M. (2014). Karamba - a toolkit for parametric structural design. *Structural Engineering International*. (Cited on page 28).

Rizzo, F., D'Asdia, P., & Lazzari, M. (2009). *Aerodynamic behaviour of hyperbolic paraboloid shaped*. Florence. (Cited on pages 35, 36).

Rizzo, F., D'Asdia, P., Ricciardelli, F., & Bartoli, G. (2012). Characterisation of pressure coefficients on hyperbolic paraboloid roofs. *Journal of Wind Engineering and Industrial Aerodynamics*. (Cited on pages 32, 37).

Schodek, D. & Bechthold, M. (2014). *Structures*. Pearson Education Limited. (Cited on page 17).

SIMULIA, D., ABAQUS 6.14. (2017). *6.4 example: Cargo crane*. Retrieved from http://129.97.46.200:2080/v6.14/. (Cited on page 30)

Suzuki, M., Sanada, S., Hayami, Y., & Ban, S. (1997). Prediction of wind-induced response of a semi-rigid haning roof. *Journal of Wind Engineering and Industrial Aerodynamics*, 357–366. (Cited on pages 35–37).

A Calculation procedure for Asymmetric Distributed Load, ULS design

Appendix A1 - Calculation procedure for Asymmetric Distributed Load, ULS design

In this Appendix the calculation procedure for the ULS design of glulam ribbons is presented for the case when the span length is equal to 24 m. The design is performed according to Eurocode.

A1.1 Geometry

Span length $l := 24\ \mathrm{m}$

Span width $B := 8\ \mathrm{m}$

Ribbon spacing $c := 0.8\ \mathrm{m}$

Initial sag $f := 2.5\ \mathrm{m}$

Assumed SR cross-section $b := 78\ \mathrm{mm}$ $h := 180\ \mathrm{mm}$ $A_{cs} := b \cdot h = 0.014\ \mathrm{m}^2$

Moment of inertia $I_y := \dfrac{b \cdot h^3}{12} = \left(3.791 \cdot 10^{-5}\right)\ \mathrm{m}^4$

A1.2 Material Properties

SR material Glulam GL30h

Density $\rho_{g.mean} := 4.8\ \dfrac{\mathrm{kN}}{\mathrm{m}^3}$

Partial factor for glulam $\gamma_{M.g} := 1.25$

Service class 1

Load duration Medium term action

Modification factor for load duration and service class $k_{mod} := 0.8$

Creep factor $k_{def} := 0$ (Creep not considered)

Factor for quasi-permanent snow load $\psi_{2.s} := 0.2$

Characteristic mean modulus of elasticity parallel to fibre $E_{0.g.mean} := 13.6\ \mathrm{GPa}$

Final char. mean modulus of elasticity parallel to fibre $E_{0.g.mean.fin} := \dfrac{E_{0.g.mean}}{1 + \psi_{2.s} \cdot k_{def}} = 13.6\ \mathrm{GPa}$

Design mean modulus of elasticity parallel to fibre

$$E_{0.g.d} := \frac{E_{0.g.mean.fin}}{\gamma_{M.g}} = 10.88 \text{ GPa}$$

Size factor for tensile strength

$$k_{h.t} := \begin{array}{l} \text{if } b < 600 \text{ mm} \\ \quad \left\| \; min\left(\left(\frac{600 \text{ mm}}{b}\right)^{0.1}, 1.1\right) \right. \\ \text{else} \\ \quad \left\| \; 1 \right. \end{array} = 1.1$$

Characteristic tensile strength parallel to fibres

$$f_{t.0.g.k} := 24 \text{ MPa}$$

Design tensile strength parallel to fibres

$$f_{t.0.g.d} := k_{mod} \cdot k_{h.t} \frac{f_{t.0.g.k}}{\gamma_{M.g}} = 16.896 \text{ MPa}$$

Size factor for bending strength

$$k_{h.m} := \begin{array}{l} \text{if } h < 600 \text{ mm} \\ \quad \left\| \; min\left(\left(\frac{600 \text{ mm}}{h}\right)^{0.1}, 1.1\right) \right. \\ \text{else} \\ \quad \left\| \; 1 \right. \end{array} = 1.1$$

Characteristic bending strength

$$f_{m.g.k} := 30 \text{ MPa}$$

Design bending strength

$$f_{m.g.d} := k_{mod} \cdot k_{h.m} \frac{f_{m.g.k}}{\gamma_{M.g}} = 21.12 \text{ MPa}$$

A1.3 Loads

A1.3.1 Self-weight

SR self-weight

$$g_{k.SR} := \rho_{g.mean} \cdot A_{cs} = 0.067 \ \frac{\text{kN}}{\text{m}}$$

Additional self-weight (sheeting etc.)

$$g_{k.add} := 1 \ \frac{\text{kN}}{\text{m}^2} \cdot c = 0.8 \ \frac{\text{kN}}{\text{m}}$$

Total characteristic self-weight

$$g_k := g_{k.SR} + g_{k.add} = 0.867 \ \frac{\text{kN}}{\text{m}}$$

A1.3.2 Snow load

Characteristic snow load $s_k := 2.0\ \frac{\text{kN}}{\text{m}^2} \cdot c = 1.6\ \frac{\text{kN}}{\text{m}}$

Snow shape factor $\mu_1 := 1.0$

Factor for combination value of snow $\psi_{0.s} := 0.7$

A1.3.3 Load combination

Security factor $\gamma_d := 1.0$

Total design load (eq. 6.10a) $q_{d.6.10a} := \gamma_d \cdot \left(1.35\ g_k + 1.5\ \psi_{0.s} \cdot \mu_1 \cdot s_k\right) = 2.851\ \frac{\text{kN}}{\text{m}}$

Total design load (eq. 6.10b) $q_{d.6.10b} := \gamma_d \cdot \left(0.89 \cdot 1.35\ g_k + 1.5\ \mu_1 \cdot s_k\right) = 3.442\ \frac{\text{kN}}{\text{m}}$

Design self-weight

$$G_d := \begin{array}{l} \text{if } q_{d.6.10a} \ge q_{d.6.10b} \\ \quad \| \ \gamma_d \cdot 1.35\ g_k \\ \text{else} \\ \quad \| \ \gamma_d \cdot 0.89 \cdot 1.35\ g_k \end{array} = 1.042\ \frac{\text{kN}}{\text{m}}$$

Design imposed load

$$Q_d := \begin{array}{l} \text{if } q_{d.6.10a} \ge q_{d.6.10b} \\ \quad \| \ \gamma_d \cdot 1.5\ \psi_{0.s} \cdot \mu_1 \cdot s_k \\ \text{else} \\ \quad \| \ \gamma_d \cdot 1.5\ \mu_1 \cdot s_k \end{array} = 2.4\ \frac{\text{kN}}{\text{m}}$$

A1.4 Analysis

$$H_g := \frac{G_d \cdot l^2}{8\ f} = 0.03\ \text{MN}$$ Horizontal force from self-weight

$$\lambda(\Delta H) := \sqrt{\frac{H_g + \Delta H}{E_{0.g.d} \cdot I_y}}$$

Cable shape function $z(x) := -\frac{4\ f}{l^2}\ x^2 + \frac{4\ f}{l}\ x$

First derivative of cable shape function $z'(x) := -\frac{8\ f}{l^2}\ x + \frac{4\ f}{l}$

Initial guess value for ΔH $\quad \Delta H_{guess} := H_g$

Equation for calculation of horizontal force from variable load:

$$\Delta H_{guess} = \frac{\left(Q_d - 2 \cdot G_d \cdot \frac{\Delta H_{guess}}{H_g}\right) \cdot f \cdot E_{0.g.d} \cdot A_{cs}}{\left(H_g + \Delta H_{guess}\right)} \cdot \left(\frac{1}{3} - \frac{4}{\left(\lambda\left(\Delta H_{guess}\right) \cdot l\right)^2} + \frac{8 \cdot tanh\left(\frac{\lambda\left(\Delta H_{guess}\right) \cdot l}{2}\right)}{\left(\lambda\left(\Delta H_{guess}\right) \cdot l\right)^3}\right)$$

Horizontal force from variable load $\quad \Delta H := \mathbf{find}\left(\Delta H_{guess}\right) = 0.034\ \text{MN}$

Redefinition of factor λ: $\quad \lambda := \lambda\left(\Delta H\right)$

Total horizontal load: $\quad H := H_g + \Delta H = 64.296\ \text{kN}$

Constants:

$$c_1 := \frac{\left(Q_d - G_d \cdot \frac{\Delta H}{H_g}\right)\left(\frac{l^2}{8} - \frac{2}{\lambda^2}\right) - \frac{l^2}{8}\ G_d \cdot \frac{\Delta H}{H_g}}{2\ \left(H_g + \Delta H\right)} = -0.11\ \text{m}$$

$$c_2 := \frac{-Q_d \cdot l}{8\ \left(H_g + \Delta H\right)} = -0.112$$

$$c_3 := \frac{Q_d \cdot \left(\cosh\left(\frac{\lambda \cdot l}{2}\right) + 1\right) - 2 \cdot G_d \cdot \frac{\Delta H}{H_g}}{2\ \left(H_g + \Delta H\right) \cdot \lambda^2 \cdot \cosh\left(\frac{\lambda \cdot l}{2}\right)} = 0.12\ \text{m}$$

$$c_4 := \frac{Q_d \cdot \left(\cosh\left(\frac{\lambda \cdot l}{2}\right) - 1\right)}{2\ \left(H_g + \Delta H\right) \cdot \lambda^2 \cdot \sinh\left(\frac{\lambda \cdot l}{2}\right)} = 0.118\ \text{m}$$

$$c_5 := \frac{\left(Q_d - 2\ G_d \cdot \frac{\Delta H}{H_g}\right)\frac{l^2}{8} + \frac{2}{\lambda^2}\ G_d \cdot \frac{\Delta H}{H_g}}{2\ \left(H\right)} = 0.13\ \text{m}$$

$$c_6 := c_2$$

$$c_7 := \frac{-Q_d \cdot \left(\cosh\left(\frac{\lambda \cdot l}{2}\right) - 1\right) - 2 \cdot G_d \cdot \frac{\Delta H}{H_g}}{2\left(H_g + \Delta H\right) \cdot \lambda^2 \cdot \cosh\left(\frac{\lambda \cdot l}{2}\right)} = -0.12 \text{ m}$$

$$c_8 := c_4$$

Deflection:

$$w_1(x) := c_1 + c_2 \cdot x + c_3 \cdot \cosh(\lambda \cdot x) + c_4 \cdot \sinh(\lambda \cdot x) - \frac{Q_d - G_d \cdot \frac{\Delta H}{H_g}}{2\left(H_g + \Delta H\right)} \cdot x^2$$

$$w_2(x) := c_5 + c_6 \cdot x + c_7 \cdot \cosh(\lambda \cdot x) + c_8 \cdot \sinh(\lambda \cdot x) + \frac{G_d \cdot \frac{\Delta H}{H_g}}{2\left(H_g + \Delta H\right)} \cdot x^2$$

First two derivatives of the deflection:

$$w'_1(x) := c_2 + \lambda \cdot c_3 \cdot \sinh(\lambda \cdot x) + \lambda \cdot c_4 \cdot \cosh(\lambda \cdot x) - \frac{Q_d - G_d \cdot \frac{\Delta H}{H_g}}{\left(H_g + \Delta H\right)} \cdot x$$

$$w''_1(x) := \lambda^2 \cdot c_3 \cdot \cosh(\lambda \cdot x) + \lambda^2 \cdot c_4 \cdot \sinh(\lambda \cdot x) + \frac{\Delta H \cdot G_d - H_g \cdot Q_d}{\Delta H \cdot H_g + {H_g}^2}$$

$$w'_2(x) := c_6 + \lambda \cdot c_7 \cdot \sinh(\lambda \cdot x) + \lambda \cdot c_8 \cdot \cosh(\lambda \cdot x) + \frac{G_d \cdot \frac{\Delta H}{H_g}}{\left(H_g + \Delta H\right)} \cdot x$$

$$w''_2(x) := \lambda^2 \cdot c_7 \cdot \cosh(\lambda \cdot x) + \lambda^2 \cdot c_8 \cdot \sinh(\lambda \cdot x) + \frac{G_d \cdot \frac{\Delta H}{H_g}}{\left(H_g + \Delta H\right)}$$

A1.5 Results

Part 1, with imposed load

Bending moment in SR $M_1(x) := -E_{0.g.d} \cdot I_y \cdot w''_1(x)$

Normal force in SR $N_1(x) := H\sqrt{1+\left(z'(x)+w'_1(x)\right)^2}$

Design bending moment in SR $M_{Ed.SR.1} := M_1(-6\ \mathrm{m}) = 6.33\ \mathrm{kN \cdot m}$

Design normal force in SR $N_{Ed.SR.1} := N_1\left(-\frac{l}{2}\right) = 86.514\ \mathrm{kN}$

Design bending stress $\sigma_{m.y.d.1} := \frac{M_{Ed.SR.1}}{I_y} \frac{h}{2} = 15.018\ \mathrm{MPa}$

Design tensile stress $\sigma_{t.0.d.1} := \frac{N_{Ed.SR.1}}{A_{cs}} = 6.162\ \mathrm{MPa}$

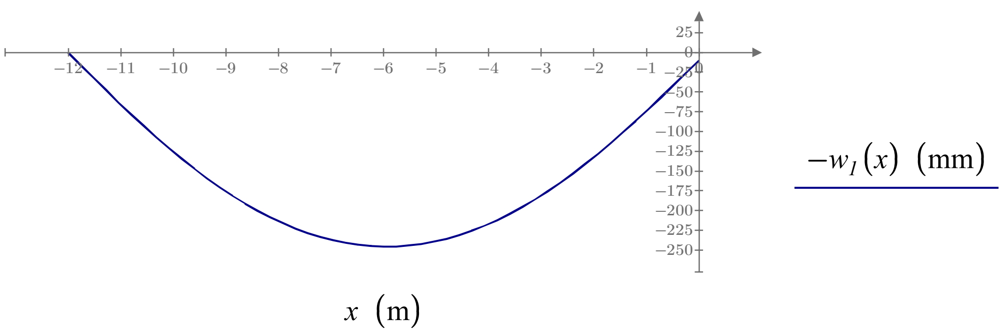

Figure A1.1 Deflection of SR.

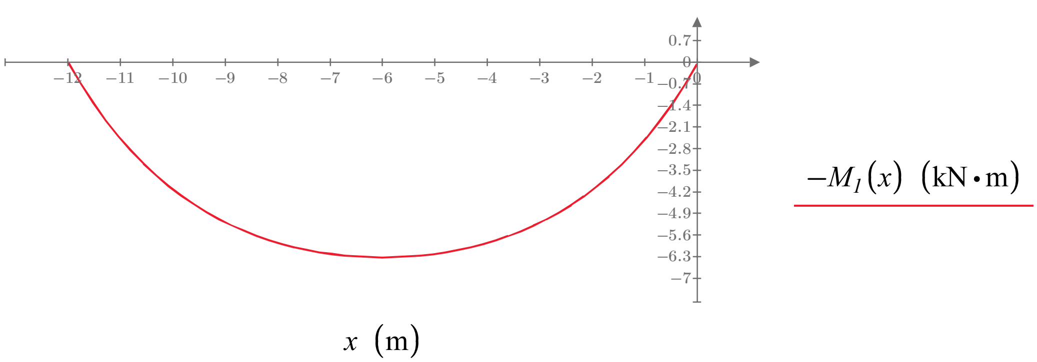

Figure A1.2 Moment distribution of SR.

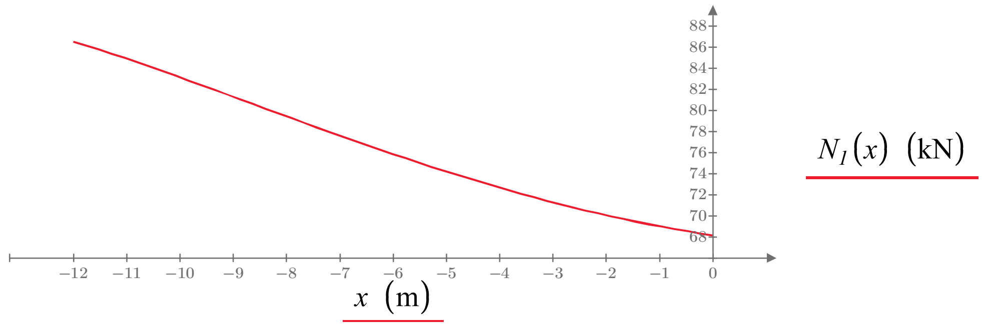

Figure A1.3 Normal force of SR.

Part 2, without imposed load:

Bending moment in SR	$M_2(x) := -E_{0.g.d} \cdot I_y\ w''_2(x)$
Normal force in SR	$N_2(x) := H \sqrt{1 + \left(z'(x) + w'_2(x)\right)^2}$
Design bending moment in SR	$M_{Ed.SR.2} := M_2(6\ \text{m}) = -6.21\ \text{kN} \cdot \text{m}$
Design normal force in SR	$N_{Ed.SR.2} := N_2(0\ \text{m}) = 68.144\ \text{kN}$
Design bending stress	$\sigma_{m.y.d.2} := \dfrac{M_{Ed.SR.2}}{I_y} \dfrac{h}{2} = -14.751\ \text{MPa}$
Design tensile stress	$\sigma_{t.0.d.2} := \dfrac{N_{Ed.SR.2}}{A_{cs}} = 4.854\ \text{MPa}$

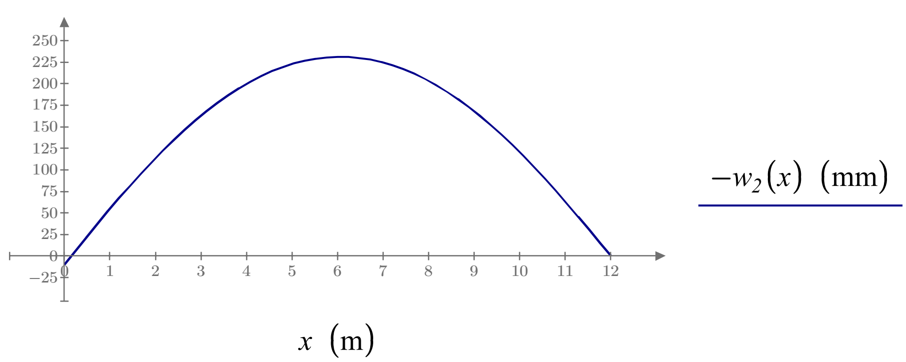

Figure A1.4 Deflection of SR.

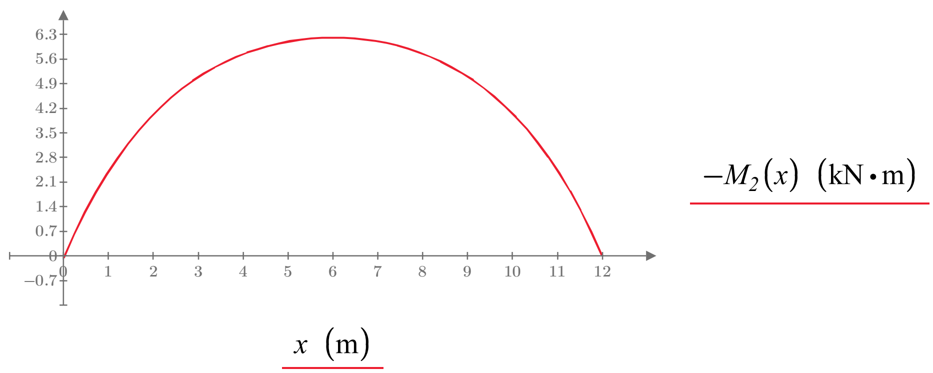

Figure A1.5 Moment distribution of SR.

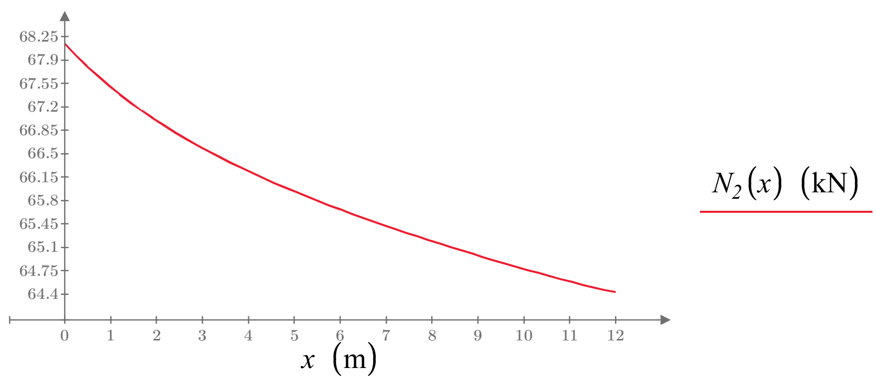

Figure A1.6 Normal force of SR.

B Calculation procedure for a Central Point Load, ULS design

B1 - Calculation procedure for a Central Point Load, ULS design

In this Appendix the calculation procedure for the ULS design of glulam ribbons is presented for the case when the span length is equal to 24 m. The design is performed according to Eurocode.

B1.1 Geometry

Span length	$l := 24\ \text{m}$
Span width	$B := 8\ \text{m}$
Ribbon spacing	$c := 0.8\ \text{m}$
Initial sag	$f := 2.5\ \text{m}$
Assumed SR cross-section	$b := 78\ \text{mm}$ $\quad h := 180\ \text{mm}$ $\quad A_{cs} := b \cdot h = 0.014\ \text{m}^2$
Moment of inertia	$I_y := \dfrac{b \cdot h^3}{12} = \left(3.791 \cdot 10^{-5}\right)\ \text{m}^4$

B1.2 Material Properties

SR material	Glulam GL30h
Density	$\rho_{g.mean} := 4.8\ \dfrac{\text{kN}}{\text{m}^3}$
Partial factor for glulam	$\gamma_{M.g} := 1.25$
Service class	1
Load duration	Medium term action
Modification factor for load duration and service class	$k_{mod} := 0.8$
Creep factor	$k_{def} := 0$ (Creep not considered)
Factor for quasi-permanent snow load	$\psi_{2.s} := 0.2$
Characteristic mean modulus of elasticity parallel to fibre	$E_{0.g.mean} := 13.6\ \text{GPa}$

Final char. mean modulus of elasticity parallel to fibre

$$E_{0.g.mean.fin} := \frac{E_{0.g.mean}}{1 + \psi_{2.s} \cdot k_{def}} = 13.6 \text{ GPa}$$

Design mean modulus of elasticity parallel to fibre

$$E_{0.g.d} := \frac{E_{0.g.mean.fin}}{\gamma_{M.g}} = 10.88 \text{ GPa}$$

Size factor for tensile strength

$$k_{h.t} := \text{if } b < 600 \text{ mm} \;\; \left\| \; min\left(\left(\frac{600 \text{ mm}}{b}\right)^{0.1}, 1.1\right) \right. \;\; \text{else} \;\; \| \; 1 \qquad = 1.1$$

Characteristic tensile strength parallel to fibres

$$f_{t.0.g.k} := 24 \text{ MPa}$$

Design tensile strength parallel to fibres

$$f_{t.0.g.d} := k_{mod} \cdot k_{h.t} \frac{f_{t.0.g.k}}{\gamma_{M.g}} = 16.896 \text{ MPa}$$

Size factor for bending strength

$$k_{h.m} := \text{if } h < 600 \text{ mm} \;\; \left\| \; min\left(\left(\frac{600 \text{ mm}}{h}\right)^{0.1}, 1.1\right) \right. \;\; \text{else} \;\; \| \; 1 \qquad = 1.1$$

Characteristic bending strength

$$f_{m.g.k} := 30 \text{ MPa}$$

Design bending strength

$$f_{m.g.d} := k_{mod} \cdot k_{h.m} \frac{f_{m.g.k}}{\gamma_{M.g}} = 21.12 \text{ MPa}$$

B1.3 Loads

B1.3.1 Self-weight

SR self-weight

$$g_{k.SR} := \rho_{g.mean} \cdot A_{cs} = 0.067 \ \frac{\text{kN}}{\text{m}}$$

Additional self-weight (sheeting etc.)

$$g_{k.add} := 1 \ \frac{\text{kN}}{\text{m}^2} \cdot c = 0.8 \ \frac{\text{kN}}{\text{m}}$$

Total characteristic self-weight

$$g_k := g_{k.SR} + g_{k.add} = 0.867 \ \frac{\text{kN}}{\text{m}}$$

B1.3.2 Snow load

Characteristic snow load $s_k := 2.0 \ \frac{\text{kN}}{\text{m}^2} \cdot c = 1.6 \ \frac{\text{kN}}{\text{m}}$

Snow shape factor $\mu_1 := 1.0$

Factor for combination value of snow $\psi_{0.s} := 0.7$

B1.3.3 Load combination

Security factor $\gamma_d := 1.0$

Total design load (eq. 6.10a) $q_{d.6.10a} := \gamma_d \cdot \left(1.35 \ g_k + 1.5 \ \psi_{0.s} \cdot \mu_1 \cdot s_k\right) = 2.851 \ \frac{\text{kN}}{\text{m}}$

Total design load (eq. 6.10b) $q_{d.6.10b} := \gamma_d \cdot \left(0.89 \cdot 1.35 \ g_k + 1.5 \ \mu_1 \cdot s_k\right) = 3.442 \ \frac{\text{kN}}{\text{m}}$

Design self-weight

$$G_d := \begin{array}{|l} \text{if } q_{d.6.10a} \geq q_{d.6.10b} \\ \quad \| \ \gamma_d \cdot 1.35 \ g_k \\ \text{else} \\ \quad \| \ \gamma_d \cdot 0.89 \cdot 1.35 \ g_k \end{array} = 1.042 \ \frac{\text{kN}}{\text{m}}$$

Design imposed load

$$Q_d := \begin{array}{|l} \text{if } q_{d.6.10a} \geq q_{d.6.10b} \\ \quad \| \ \gamma_d \cdot 1.5 \ \psi_{0.s} \cdot \mu_1 \cdot s_k \cdot c \\ \text{else} \\ \quad \| \ \gamma_d \cdot 1.5 \ \mu_1 \cdot s_k \cdot c \end{array} = 1.92 \ \text{kN}$$

B1.4 Analysis

$H_g := \frac{G_d \cdot l^2}{8 \ f} = 0.03 \ \text{MN}$ Horizontal force from self-weight

$$\lambda(\Delta H) := \sqrt{\frac{H_g + \Delta H}{E_{0.g.d} \cdot I_y}}$$

Cable shape function $z(x) := -\frac{4 \ f}{l^2} \ x^2 + \frac{4 \ f}{l} \ x$

First derivative of cable shape function $z'(x) := -\frac{8 \ f}{l^2} \ x + \frac{4 \ f}{l}$

Initial guess value for ΔH $\qquad \Delta H_{guess} := H_g$

Equation for calculation of horizontal force from variable load:

$$\Delta H_{guess} = \frac{16 \cdot f \cdot E_{0.g.d} \cdot A_{cs}}{\left(H_g + \Delta H_{guess}\right)} \cdot \left(\frac{Q_d}{l} \left(\frac{1}{16} - \frac{1}{2\left(\lambda\left(\Delta H_{guess}\right) \cdot l\right)^2} + \frac{1}{2\left(\lambda\left(\Delta H_{guess}\right) \cdot l\right)^2 \cdot cosh\left(\frac{\lambda\left(\Delta H_{guess}\right) \cdot l}{2}\right)} \right) - G_d \cdot \frac{\Delta H_{guess}}{H_g} \left(\frac{1}{24} - \frac{1}{2\left(\lambda\left(\Delta H_{guess}\right) \cdot l\right)^2} + \frac{tanh\left(\frac{\lambda\left(\Delta H_{guess}\right) \cdot l}{2}\right)}{\left(\lambda\left(\Delta H_{guess}\right) \cdot l\right)^3} \right) \right)$$

Horizontal force from central point load $\qquad \Delta H := \mathbf{find}\left(\Delta H_{guess}\right) = 0.004 \text{ MN}$

Redefinition of factor λ: $\qquad \lambda := \lambda\left(\Delta H\right) = 0.285 \ \frac{1}{\text{m}}$

Total horizontal load: $\qquad H := H_g + \left(\Delta H\right) = 33.546 \text{ kN}$

Constants:

$$c_1 := \frac{Q_d \cdot \frac{l}{4} - G_d \cdot \frac{\Delta H}{H_g} \cdot \left(\frac{l^2}{8} - \frac{1}{\lambda^2}\right)}{2 \cdot \left(H_g + \Delta H\right)} = 0.063 \text{ m}$$

$$c_2 := \frac{-Q_d}{2 \cdot \left(H_g + \Delta H\right)} = -0.029$$

$$c_3 := -\frac{\frac{Q_d}{2\,\lambda} \cdot \sinh\left(\frac{\lambda \cdot l}{2}\right) + \frac{G_d}{\lambda^2} \cdot \frac{\Delta H}{H_g}}{\left(H_g + \Delta H\right) \cdot \cosh\left(\frac{\lambda \cdot l}{2}\right)} = -0.103 \text{ m}$$

$$c_4 := \frac{Q_d}{2\,\lambda \cdot \left(H_g + \Delta H\right)} = 0.1 \text{ m}$$

Deflection:

Particular solution for the deflection: $\qquad w_{part}(x) := \frac{\Delta H \cdot G_d \cdot x^2}{2 \cdot H_g \cdot \left(H_g + \Delta H\right)}$

$$w(x) := c_1 + c_2 \cdot x + c_3 \cdot \cosh(\lambda \cdot x) + c_4 \cdot \sinh(\lambda \cdot x) + w_{part}(x)$$

First three derivatives of the deflection:

$$w'(x) := c_2 + \lambda \cdot c_3 \cdot \sinh(\lambda \cdot x) + \lambda \cdot c_4 \cdot \cosh(\lambda \cdot x) + \frac{\Delta H \cdot G_d \cdot x}{H_g \cdot (H_g + \Delta H)}$$

$$w''(x) := \lambda^2 \cdot c_3 \cdot \cosh(\lambda \cdot x) + \lambda^2 \cdot c_4 \cdot \sinh(\lambda \cdot x) + \frac{\Delta H \cdot G_d}{H_g \cdot (H_g + \Delta H)}$$

$$w'''(x) := \lambda^3 \cdot c_3 \cdot \sinh(\lambda \cdot x) + \lambda^3 \cdot c_4 \cdot \cosh(\lambda \cdot x)$$

Part 1

The chart in Part 1 will be symmetrical for Part 2.

Normal force in SR	$N(x) := H \sqrt{1 + (z'(x) + w'(x))^2}$
Bending moment in SR	$M(x) := -E_{0.g.d} \cdot I_y \, w''(x)$
Design normal force in SR	$N_{Ed.SR} := N(0 \text{ m}) = 36.342 \text{ kN}$
Design bending moment in SR	$M_{Ed.SR} := M(0 \text{ m}) = 1.95 \text{ kN} \cdot \text{m}$
Design tensile stress	$\sigma_{t.0.d.1} := \frac{N_{Ed.SR}}{A_{cs}} = 2.588 \text{ MPa}$
Design bending stress	$\sigma_{m.yd} := \frac{M_{Ed.SR}}{I_y} \cdot \frac{h}{2} = 4.629 \text{ MPa}$

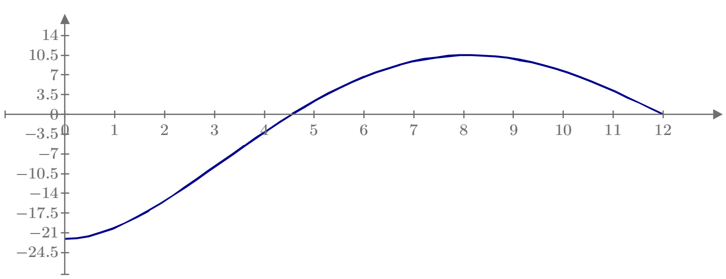

$-w(x)$ (mm)

x (m)

Figure B1.1 Deflection of SR.

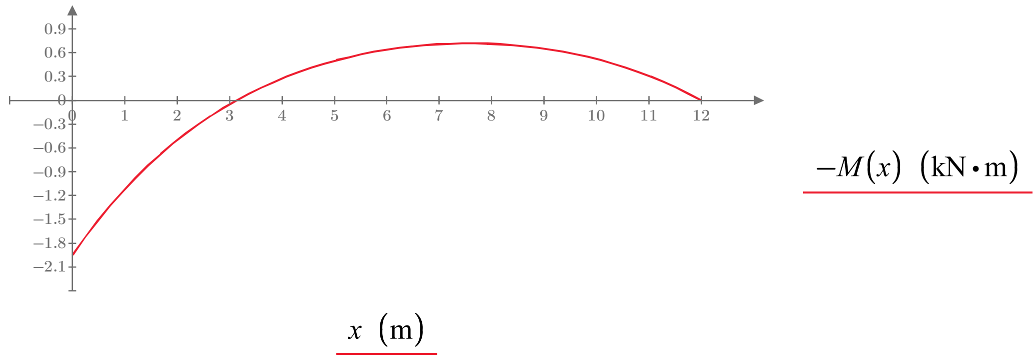

Figure B1.2 Moment distribution of SR.

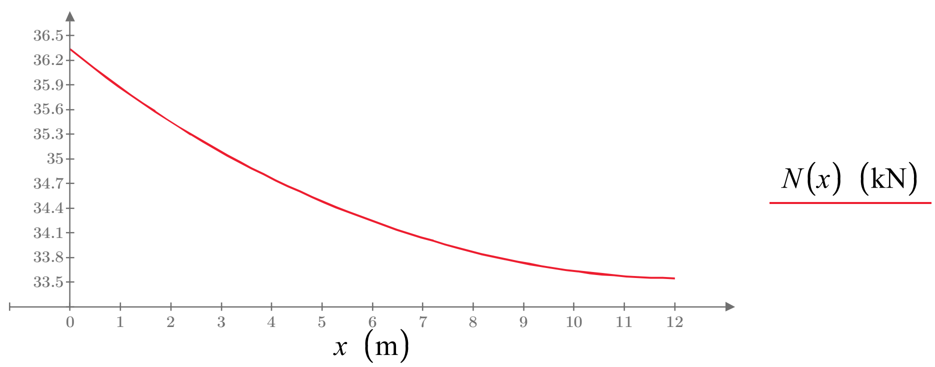

Figure B1.3 Normal force distribution of SR.

C Caluculation of imposed loads

C1 - Calculation of imposed loads

In this appendix, the affect on the roof caused by the wind- and snow load will be presented. The design procedure is performed according to Eurocode.

C1.1 Geometry

Span length	$l := 24\ \text{m}$		
Span width	$B := 8\ \text{m}$		
Ribbon spacing	$c := 0.8\ \text{m}$		
Initial sag	$f := 2.5\ \text{m}$		
Assumed SR cross-section	$b_{gl30h} := 78\ \text{mm}$	$h_{gl30h} := 180\ \text{mm}$	$A_{cs.gl30h} := b_{gl30h} \cdot h_{gl30h} = 0.014\ \text{m}^2$
Assumed area of the plywood	$b_{ply} := 800\ \text{mm}$	$h_{ply} := 12\ \text{mm}$	$A_{ply} := b_{ply} \cdot h_{ply} = 0.01\ \text{m}^2$
Assumed area of the insulation	$b_{ply} := 0.8\ \text{m}$	$h_{ins} := 300\ \text{mm}$	$A_{ins} := b_{ply} \cdot h_{ins} = 0.24\ \text{m}^2$
Moment of inertia of the SR	$I_y := \dfrac{b_{gl30h} \cdot h_{gl30h}^{\ 3}}{12} = \left(3.791 \cdot 10^{-5}\right)\ \text{m}^4$		

C1.2 Material Properties

SR material	Glulam GL30h
Density:	
Glulam	$\rho_{g.mean.Gl30h} := 4.8\ \dfrac{\text{kN}}{\text{m}^3}$
Plywood	$\rho_{g.mean.ply} := 5.5\ \dfrac{\text{kN}}{\text{m}^3}$
Insulation	$\rho_{g.mean.ins} := 0.35\ \dfrac{\text{kN}}{\text{m}^3}$
Partial factor for glulam	$\gamma_{M.g} := 1.25$
Service class	1
Load duration	Medium term action
Modification factor for load duration and service class	$k_{mod} := 0.8$
Creep factor	$k_{def} := 0$ (Creep not considered)
Factor for quasi-permanent snow load	$\psi_{2.s} := 0.2$
Characteristic mean modulus of elasticity parallel to fibre	$E_{0.g.mean} := 13.6\ \text{GPa}$

Final char. mean modulus of elasticity parallel to fibre

$$E_{0.g.mean.fin} := \frac{E_{0.g.mean}}{1 + \psi_{2.s} \cdot k_{def}} = 13.6\ \text{GPa}$$

Design mean modulus of elasticity parallel to fibre

$$E_{0.g.d} := \frac{E_{0.g.mean.fin}}{\gamma_{M.g}} = 10.88\ \text{GPa}$$

Size factor for tensile strength

$$k_{h.t} := \begin{cases} \min\left(\left(\dfrac{600\ \text{mm}}{b_{gl30h}}\right)^{0.1}, 1.1\right) & \text{if } b_{gl30h} < 600\ \text{mm} \\ 1 & \text{else} \end{cases}$$

Characteristic tensile strength parallel to fibres

$$f_{t.0.g.k} := 24\ \text{MPa}$$

Design tensile strength parallel to fibres

$$f_{t.0.g.d} := k_{mod} \cdot k_{h.t}\ \frac{f_{t.0.g.k}}{\gamma_{M.g}} = 16.896\ \text{MPa}$$

Size factor for bending strength

$$k_{h.m} := \begin{cases} \min\left(\left(\dfrac{600\ \text{mm}}{h_{gl30h}}\right)^{0.1}, 1.1\right) & \text{if } h_{gl30h} < 600\ \text{mm} \\ 1 & \text{else} \end{cases} = 1.1$$

Characteristic bending strength

$$f_{m.g.k} := 30\ \text{MPa}$$

Design bending strength

$$f_{m.g.d} := k_{mod} \cdot k_{h.m}\ \frac{f_{m.g.k}}{\gamma_{M.g}} = 21.12\ \text{MPa}$$

C1.3 Loads

C1.3.1 Self-weight

SR self-weight $g_{k.SR} := \rho_{g.mean.Gl30h} \cdot A_{cs.gl30h} = 0.067 \ \frac{kN}{m}$

Plywood self-weight, (3 layers) $g_{k.ply} := 3 \cdot \rho_{g.mean.ply} \cdot A_{ply} = 0.158 \ \frac{kN}{m}$

Insultation self-weight $g_{k.ins} := \rho_{g.mean.ins} \cdot A_{ins} = 0.084 \ \frac{kN}{m}$

Cladding self-weight , (2-layer roof paper) $g_{cladding} := 0.036 \ \frac{kN}{m^2}$

$g_{cladding.tot} := 2 \cdot g_{cladding} \cdot c = 0.058 \ \frac{kN}{m}$

Installation self-weight $g_{installation} := 0.5 \ \frac{kN}{m^2}$

$g_{installation.tot} := g_{installation} \cdot c = 0.4 \ \frac{kN}{m}$

Total Self-weight $g_{k.SR.tot} := g_{k.SR} + g_{k.ply} + g_{k.ins} + g_{cladding.tot} + g_{installation.tot} = 0.767 \ \frac{kN}{m}$

C1.3.2 Wind load

Terrain category: III
Height of building: z = 15m $c_e := 2$

Reference wind speed: $v_b := 24 \ \frac{m}{s}$

Reference mean velocity pressure: $q_b := \frac{v_b^{\,2}}{1600 \ \frac{m^2}{s^2}} \cdot \frac{kN}{m^2} = 0.36 \ \frac{kN}{m^2}$

Peak velocity pressure: $q_p := c_e \cdot q_b = 0.72 \ \frac{kN}{m^2}$

External wind coefficients value, hyperbolic paraboloid roof, Alt (a)

$c_{pe1} := -1.3$
$c_{pe2} := -1$
$c_{pe3} := -0.8$

Internal wind coefficients according to EC1: $c_{pi} := -0.2$

External pressure: $w_1 := q_p \cdot (c_{pe1} + c_{pi}) \cdot c = -0.864\ \frac{\text{kN}}{\text{m}}$

$w_2 := q_p \cdot (c_{pe2} + c_{pi}) \cdot c = -0.691\ \frac{\text{kN}}{\text{m}}$

$w_3 := q_p \cdot (c_{pe3} + c_{pi}) \cdot c = -0.576\ \frac{\text{kN}}{\text{m}}$

C1.3.3 Snow load

Snow zone: Stockholm $s_k := 2\ \frac{\text{kN}}{\text{m}^2}$

Roof slope: $\alpha_1 := 22\ \text{deg}$

$\alpha_2 := 22\ \text{deg}$

Shape coefficient (22 °): $\mu_1 := 0.8$

$\mu_2 := 1.4$

Characteristic value of snow load: $S_1 := s_k \cdot \mu_1 \cdot c = 1.28\ \frac{\text{kN}}{\text{m}}$

$S_2 := s_k \cdot \mu_2 \cdot c = 2.24\ \frac{\text{kN}}{\text{m}}$

Factor for combination value of snow $\psi_{0.s} := 0.7$

C1.4 Load combination

C1.4.1 Load combination - Wind load

Load combinations for wind load: EQU eq. 6.10 - EC1, favourable action, ULS

Design self-weight $G_{d.wind.ULS} := g_{k.SR.tot} \cdot 0.9 = 0.691\ \frac{\text{kN}}{\text{m}}$

Design wind load: $Q_{d.wind.ULS.1} := w_1 \cdot 1.5 = -1.296\ \frac{\text{kN}}{\text{m}}$

$Q_{d.wind.ULS.2} := w_2 \cdot 1.5 = -1.037\ \frac{\text{kN}}{\text{m}}$

$Q_{d.wind.ULS.3} := w_3 \cdot 1.5 = -0.864\ \frac{\text{kN}}{\text{m}}$

Load combinations for wind load: EQU eq. 6.14b , SLS

Design self-weight $G_{d.wind.SLS} := g_{k.SR.tot} = 0.767\ \frac{kN}{m}$

Design wind load: $Q_{d.wind.SLS.1} := w_1 = -0.864\ \frac{kN}{m}$

$Q_{d.wind.SLS.2} := w_2 = -0.691\ \frac{kN}{m}$

$Q_{d.wind.SLS.3} := w_3 = -0.576\ \frac{kN}{m}$

C1.4.2 Load combination - Snow load

C1.4.2.1 Uniform distributed snow load (alternative 1), ULS design

Security factor $\gamma_d := 1.0$

Total design load (eq. 6.10a) $q_{d.6.10a.1.ULS} := \gamma_d \cdot \left(1.35\ g_{k.SR.tot} + 1.5\ \psi_{0.s} \cdot S_1\right) = 2.38\ \frac{kN}{m}$

Total design load (eq. 6.10b) $q_{d.6.10b.1.ULS} := \gamma_d \cdot \left(0.89 \cdot 1.35\ g_{k.SR.tot} + 1.5\ S_1\right) = 2.842\ \frac{kN}{m}$

Design self-weight

$$G_{d.1} := \begin{aligned} & \text{if } q_{d.6.10a.1.ULS} \ge q_{d.6.10b.1.ULS} \\ & \quad \gamma_d \cdot 1.35\ g_{k.SR.tot} \\ & \text{else} \\ & \quad \gamma_d \cdot 0.89 \cdot 1.35\ g_{k.SR.tot} \end{aligned} = 0.922\ \frac{kN}{m}$$

Design imposed load

$$Q_{d.1} := \begin{aligned} & \text{if } q_{d.6.10a.1.ULS} \ge q_{d.6.10b.1.ULS} \\ & \quad \gamma_d \cdot 1.5\ \psi_{0.s} \cdot S_1 \\ & \text{else} \\ & \quad \gamma_d \cdot 1.5\ S_1 \end{aligned} = 1.92\ \frac{kN}{m}$$

C1.4.2.2 Triangular shaped snow load (alternative 2), ULS design

Security factor $\gamma_d := 1.0$

Total design load (eq. 6.10a) $q_{d.6.10a.2.ULS} := \gamma_d \cdot \left(1.35\ g_{k.SR.tot} + 1.5\ \psi_{0.s} \cdot S_2\right) = 3.388\ \frac{kN}{m}$

Total design load (eq. 6.10b) $q_{d.6.10b.2.ULS} := \gamma_d \cdot \left(0.89 \cdot 1.35\ g_{k.SR.tot} + 1.5\ S_2\right) = 4.282\ \frac{kN}{m}$

Design self-weight
$$G_{d.snow.2.ULS} := \begin{array}{l} \text{if } q_{d.6.10a.2.ULS} \geq q_{d.6.10b.2.ULS} \\ \quad \| \gamma_d \cdot 1.35\ g_{k.SR.tot} \\ \text{else} \\ \quad \| \gamma_d \cdot 0.89 \cdot 1.35\ g_{k.SR.tot} \end{array} = 0.922\ \frac{kN}{m}$$

Design imposed load
$$Q_{d.snow.2.ULS} := \begin{array}{l} \text{if } q_{d.6.10a.2.ULS} \geq q_{d.6.10b.2.ULS} \\ \quad \| \gamma_d \cdot 1.5\ \psi_{0.s} \cdot S_2 \\ \text{else} \\ \quad \| \gamma_d \cdot 1.5\ S_2 \end{array} = 3.36\ \frac{kN}{m}$$

C1.4.2.3 Uniform distributed snow load (alternative 1), SLS design

Load combinations for snow load: EQU eq. 6.14b , SLS

Total design load $q_{d.snow.1.SLS} := \gamma_d \cdot \left(g_{k.SR.tot} + S_1\right) = 2.047\ \frac{kN}{m}$

Design self-weight $G_{d.snow.1.SLS} := \gamma_d \cdot g_{k.SR.tot} = 0.767\ \frac{kN}{m}$

Design imposed load $Q_{d.snow.1.SLS} := \gamma_d \cdot S_1 = 1.28\ \frac{kN}{m}$

C1.4.2.4 Triangular shaped snow load (alternative 2), SLS design

Load combinations for snow load: EQU eq. 6.14b , SLS

Security factor $\gamma_d := 1.0$

Total design load $q_{d.snow.2.SLS} := \gamma_d \cdot \left(g_{k.SR.tot} + S_2\right) = 3.007\ \frac{kN}{m}$

Design self-weight $G_{d.snow.1.SLS} := \gamma_d \cdot g_{k.SR.tot} = 0.767\ \frac{kN}{m}$

Design imposed load $Q_{d.snow.1.SLS} := \gamma_d \cdot S_2 = 2.24\ \frac{kN}{m}$

D Calculation procedure of buckling load

D1 - Calculation procedure of buckling load

A check of the buckling load capacity due the uplifting force caused by the wind will be presented according to Limträhandboken, Del 2.

D1.1 Geometry

Span length $l := 24\ \text{m}$

Initial sag $f := 2.5\ \text{m}$

Assumed SR cross-section $b := 78\ \text{mm}$ $h := 180\ \text{mm}$ $A_{cs} := b \cdot h = 0.014\ \text{m}^2$

Moment of inertia $I_y := \dfrac{b \cdot h^3}{12} = \left(3.791 \cdot 10^{-5}\right)\ \text{m}^4$

D1.2 Material Properties

SR material Glulam GL30h

Density $\rho_{g.mean} := 4.8\ \dfrac{\text{kN}}{\text{m}^3}$

Partial factor for glulam $\gamma_{M.g} := 1.25$

Service class 1

Load duration Medium term action

Modification factor for load duration and service class $k_{mod} := 0.8$

Creep factor $k_{def} := 0$ (Creep not considered)

Factor for quasi-permanent snow load $\psi_{2.s} := 0.2$

Characteristic mean modulus of elasticity parallel to fibre $E_{0.g.mean} := 13.6\ \text{GPa}$

Final char. mean modulus of elasticity parallel to fibre $E_{0.g.mean.fin} := \dfrac{E_{0.g.mean}}{1 + \psi_{2.s} \cdot k_{def}} = 13.6\ \text{GPa}$

Design mean modulus of elasticity parallel to fibre $E_{0.g.d} := \dfrac{E_{0.g.mean.fin}}{\gamma_{M.g}} = 10.88\ \text{GPa}$

D1.3 Loads

Numerical factor, depending on sag and $\gamma := 25$

Critical load $q_{cr} := \gamma \cdot \frac{E_{0.g.d} \cdot I_y}{l^3} = 0.746 \ \frac{\text{kN}}{\text{m}}$

D1.3 Analysis

$$N_{cr.0.25l} := 1.04 \cdot \gamma \cdot \frac{E_{0.g.d} \cdot I_y}{8 \cdot f \cdot l} = 22.34 \ \text{kN}$$

The Normal force need to be checked with the Normal force from the FE-analysis and the following condition needs to be fulfiled: $N_{cr.0.25l} \leq N_d$

E Results gathered from analytical- and numerical solutions.

ABAQUS	1, Uniform line-load	2,Uniform node-load	3, Assymetric line-load	4, Assymetric node-load	5, Central point-load
Max Normal Force [kN]	108,5	104,5	76,8	72,8	36,75
Min Normal Force [kN]	100,3	96,7	68,37	64,8	34,2
Max Pos Moment [kNm]	0,188		5,64	5,7	1,68
Max Neg Moment [kNm]			6,12	6	0,65
Max ↓ Deflection [mm]	31,6	34,65	211,1	210,1	31,6
Max ↑ Deflection [mm]			246,4	245,1	6
Max Axial Stress [MPa]	7,73	7,44	5,47	5,19	2,62
Reaction Force [kN]	42,48	41,30	35,99/20,45	34,75/19,54	13,81

Grasshopper/Karamba	1, Uniform line-load	2,Uniform node-load	3, Assymetric line-load	4, Assymetric node-load	5, Central point-load
Max Normal Force [kN]	107,2	105,8	73,6	70,1	35,1
Min Normal Force [kN]	99	97,8	65,3	62,2	32,6
Max Pos Moment [kNm]	0,65	0,18	20,45	21,2	2,36
Max Neg Moment [kNm]			21,2	20,9	1,12
Max ↓ Deflection [mm]	41,8	30,2	828	845	42,9
Max ↑ Deflection [mm]			813	818	13,9
Max Axial Stress [MPa]	7,64	7,54	5,24	4,99	2,50
Reaction Force [kN]	41,30	41,30	34,41/20,01	34,3/19,44	13,46

Analytical Solution	1, Uniform line-load		3, Assymetric line-load		5, Central point-load
Max Normal Force [kN]	106,6		86,51		36,64
Min Normal Force [kN]	98,3		68		33,55
Max Pos Moment [kNm]	0,119		6,33		1,95
Max Neg Moment [kNm]			6,21		0,72
Max ↓ Deflection [mm]	20		245,7		23
Max ↑ Deflection [mm]			231,2		10
Max Axial Stress [MPa]	7,59		6,16		2,61
Reaction Force [kN]	41,31		34,11/19,71		13,47

F Design Proposal.

Design improvements

This proposal is based on Hofverberg (2016) design. In order to ease to production stage of connecting the timber elements, they are paired with an intermediate steel plate connected in-between the timber members. This eases the connecting of the elements on-site where no finger-joints is needed. Depending on the span-length, the timber elements needs to be manufactured in more than one piece, if the length exceeds 25 m, special permission is needed to transport the ribbons (Serrano, 2016). The disadvantages with this proposal are more material usage in the structure, due the paired ribbons.

The ribbons have a rectangular geometry with an initial curvature. The small spacing between the ribbons leads to a more material efficient construction due to the decreased section height, (Hofverberg2016). On top of the ribbons, plywood boards are nailed to the ribbons in order to increase the in-plane stiffness. More studies are needed to ensure that the plywood itself manages the horizontal loads. For installation of the steel plate in between the ribbons, bolts can be used.